

Theoretical Analysis of a Potentiostat for Studying Microbial Fuel Cells

Catarina Lousa Marques

Dissertação para obtenção do Grau de Mestre em
Engenharia Eletrotécnica e de Computadores
(2º Ciclo de Estudos)

Orientador: Professor Doutor António Eduardo Vitória do Espírito Santo

Covilhã, Outubro de 2021

Acknowledgements

To my advisor, Professor Doctor António Eduardo Vitória do Espírito Santo for accepting to guide this dissertation and for the time dispended.

To all the elements of the Instrumentation and Measurement Laboratory by the integration given, in special to Helbert for his fellowship and sympathy.

To my mother and brother for the support and calm transmitted during this phase.

To Francisco, for being an unconditional boyfriend that was always encouranging me and for being an example of dedication and effort in everything he does.

Finally, to Mariana and Daniela for the friendship and support.

Resumo

Há vários anos, que as Células de Combustível Microbianas têm sido desenvolvidas como alternativas para gerar eletricidade através da oxidação da matéria orgânica por bactérias. Embora as unidades individuais destas células tenham um baixo consumo de energia, tem-se alcançado um progresso significativo em termos de materiais e configurações das células, permitindo-lhes gerar níveis de produção mais elevados. No entanto, estas células são produzidas principalmente através de métodos de laboratório convencionais que podem levar vários meses até que as células alcancem as suas aptidões de potência máxima.

Nesta dissertação, uma abordagem para o uso de um potencióstato de baixo custo foi desenvolvida para estudar o comportamento das células de combustível microbianas. Inicialmente, o trabalho concentrou-se em estabelecer uma interface no Node-RED e fazer a ligação entre as células vivas dos reatores. Para tal, foi utilizado o microcontrolador mbed NXP LPC1768 para comunicar com a interface criada e também com o potencióstato.

De forma a explorar totalmente o potencióstato, estudamos vários testes eletroquímicos possíveis de executar no reator das células de combustível microbianas e os resultados esperados.

Por fim, pode-se dizer que o potencióstato é rápido, produz baixo ruído e é um instrumento versátil, muito promissor no estudo desta energia renovável emergente como são as células de combustível microbianas.

Palavras-chave

Células de combustível microbianas; Potencióstato; Análise eletroquímica; Voltametria cíclica; Node-RED; Mbed.

Abstract

For many years, Microbial Fuel Cells (MFCs) have been developed as alternatives for generating electricity via the oxidation of organic matter by bacteria. Even though individual MFC units are low in power, significant progress has been achieved in terms of MFC material and configurations, enabling them to generate higher output levels. Nonetheless, MFCs are mainly produced using conventional laboratory methods that can take up to several months to bring the MFCs to their maximum power aptitudes.

In this dissertation, an approach to use a low-cost potentiostat was developed in order to study MFCs comportament. Initially, the work focused on establishing an interface on Node-RED and an interconnection between the living cells in the MFC. In order to achieve that, was used a mbed NXP LPC1768 microcontroller to communicate with the interface created and also with the potentiostat.

To fully explore the potentiostat, were studied several electrochemical tests possible to execute in the MFC reactor and the expected results.

Finally, is possible to say that the potentiostat is fast, produces low noise and is a versatile instrument, very promising in the study of this emerging renewable energy like is MFCs.

Keywords

Microbial fuel cells; Potentiostat; Electrochemical analysis; Cyclic Voltammetry; Node-RED; Mbed.

Contents

| | |
|-------------------------------------------------|------|
| Acknowledgements | iii |
| Resumo | v |
| Abstract | vii |
| Contents | ix |
| List of figures | xii |
| List of tables | xv |
| List of acronyms | xvii |
| 1. Introduction | 1 |
| 1.1. Motivation | 1 |
| 1.2. Main goals | 1 |
| 1.3. Outline | 1 |
| 2. Microbial Fuel Cells | 3 |
| 2.1. Concept and evolution in the study of MFCs | 3 |
| 2.2. Biochemical process | 6 |
| 2.3. MFC components | 9 |
| 2.4. Architectures | 11 |
| 2.5. Applications | 14 |
| 3. Potentiostat | 17 |
| 3.1. Characteristics | 17 |
| 3.2. Circuit | 19 |
| 3.3. Electrochemical analysis | 20 |
| 3.4. Applications | 25 |
| 4. Study MFCs with a low-cost potentiostat | 28 |
| 4.1. Study parameters | 28 |
| 4.1.1. Electrode potential | 28 |
| 4.1.2. Power output | 29 |
| 4.1.3. Power density | 29 |
| 4.1.4. Ohmic resistance | 30 |
| 4.1.5. Polarisation curves | 31 |
| 4.1.6. Coulombic efficiency | 33 |
| 4.1.7. Loading rates | 33 |
| 4.1.8. Energy recover | 33 |
| 4.2. Study examples | 34 |
| 4.3. Dummy cells | 39 |
| | ix |

| | | |
|--------|----------------------------------------------|----|
| 5. | Potentiostat development | 40 |
| 5.1. | Circuit development and electronics assembly | 40 |
| 5.1.1. | DAC | 40 |
| 5.1.2. | ADC | 41 |
| 5.1.3. | Optical isolators | 43 |
| 5.1.4. | Potentiostat system | 44 |
| 5.2. | Functional overview of the system | 47 |
| 5.3. | Man-machine interface with Node-RED | 48 |
| 5.4. | Firmware development | 54 |
| 5.4.1. | MBED LPC1768 | 54 |
| 5.4.2. | SPI communication | 55 |
| 5.4.3. | MBED software | 55 |
| 6. | Methodology | 59 |
| 6.1. | Protocol guidelines | 59 |
| 6.2. | Simulation methodology | 60 |
| 6.2.1. | Current measurement | 60 |
| 6.2.2. | CV measurement | 61 |
| 6.2.3. | Charge/discharge measurement | 62 |
| 7. | Conclusions | 63 |
| 7.1. | Future work | 63 |
| | Bibliography | 64 |

List of figures

| | |
|------------------------------------------------------------------------------------------|----|
| Figure 2.1: Evolution graphic of MFCs research. From [3]. | 4 |
| Figure 2.2: Schematic of MFCs history. | 5 |
| Figure 2.3: System of an MFC. | 6 |
| Figure 2.4: Biochemical example. | 8 |
| Figure 2.5: One chamber reactor (left) and Two chamber reactor (right). | 12 |
| Figure 2.6: H-type MFC example | 13 |
| Figure 2.7: Schematic and picture of UMFC (adapted from [33]) | 13 |
| Figure 2.8: Chronologic order of the MFC powered autonomous robots (adapted from [10]) | 15 |
| Figure 2.9: Meteorological buoy powered by MFCs (from [34]) | 16 |
| Figure 2.10: Pee power urinal at UWE campus in 2015 (from [11]) | 16 |
| Figure 3.1: Basic potentiostat scheme | 17 |
| Figure 3.2: Potentiostat control system. | 18 |
| Figure 3.3: Potentiostat circuit. | 19 |
| Figure 3.4: Microcontroller controlled potentiostat. | 19 |
| Figure 3.5: Voltammogram example (adapted from [14]). | 21 |
| Figure 3.6: Typical voltammograms for CV (left) and LSV (right) (adapted from [15]). | 23 |
| Figure 3.7: Nyquist EIS example (adapted from [15]). | 24 |
| Figure 3.8: Photo of the potentiostat in the field (from [9]). | 26 |
| Figure 3.9: Ecostat potentiostat (from [17]). | 26 |
| Figure 3.10: Blood alcohol system (left, from [18]) and JUAMI device (right, from [20]). | 27 |
| Figure 4.1: Polarization curve (left) and Power Curve (right) (adapted from [1]). | 32 |
| Figure 4.2: Parameters studied, from [21]. | 35 |
| Figure 4.3: Schematic of a MFC type (from [22]). | 37 |
| Figure 4.4: MFCs schematic, SPA (left) and SEA (right) (from [23]). | 38 |
| Figure 4.5: Simplified schematic circuit for 3-electrode setup (from [23]). | 38 |
| Figure 4.6: Schematic diagram of a dummy cell (from [24]). | 39 |
| Figure 5.1: DAC8531 schematic. | 40 |
| Figure 5.2: ADS8331 schematic. | 42 |
| Figure 5.3: Schematic of ISO7240 and ISO7242. | 43 |
| Figure 5.4: Potentiostat system. | 44 |
| Figure 5.5: Potentiostat control circuit. | 45 |
| Figure 5.6: Electrochemical cell. | 46 |
| Figure 5.7: Overview of the setup (adapted from [29], [30], [31]). | 47 |

| | |
|----------------------------------------------------------------------------|----|
| Figure 5.8: Input parameters block in a scheme. | 48 |
| Figure 5.9: First part of the flow, relative to file saving. | 49 |
| Figure 5.10: Function blocks for global variables. | 49 |
| Figure 5.11: File result. | 50 |
| Figure 5.12: Scheme relative to Serial Port interaction in Node-RED. | 50 |
| Figure 5.13: Second part of the flow, interaction with serial port. | 51 |
| Figure 5.14: Functions of the second part of the flow. | 51 |
| Figure 5.15: Flow for the chart with x/y axis. | 52 |
| Figure 5.16: Block functions to explain the steps added. | 52 |
| Figure 5.17: Dashboard of Interface. | 53 |
| Figure 5.18: Full flow. | 53 |
| Figure 5.19: Pinout diagram of mbed NXP LPC1768 board (from [31]). | 54 |
| Figure 5.20: Diagram of mbed communications. | 55 |
| Figure 5.21: Serial Port receive event function. | 56 |
| Figure 5.22: Data acquisition routine. | 57 |
| Figure 5.23: Communication with external components. | 58 |
| Figure 6.1: Current and potential measurement example (adapted from [24]). | 60 |
| Figure 6.2: CV measurement example (adapted from [24]). | 61 |
| Figure 6.3: Triangular waveform (adapted from [24]). | 61 |
| Figure 6.4: Charge/Discharge measurement example (adapted from [24]). | 62 |

List of tables

| | |
|------------------------------------------------------------------|----|
| Table 5.1: Pin decription for DAC8531 (adapted from [25]). | 41 |
| Table 5.2: Pin description of ADS8331 (adapted from [26]). | 42 |
| Table 5.3: Pin configuration for ISO family (adapted from [27]). | 44 |
| Table 5.4: Input parameters. | 48 |
| Table 5.5: API summary for SPI Master (adapted from [31]). | 55 |

List of acronyms

| | |
|---------|---------------------------------------------|
| ADC | Analog to Digital Converter |
| Ag/Cl | Silver/Silver Chloride |
| ATP | Adenine Trisphosphate |
| BFC | Biological Fuel Cells |
| BOD | Biochemical Oxygen Demand |
| CB | Carbonate Buffer |
| CE | Counter Electrode |
| CEM | Cation Exchange Membrane |
| CV | Cyclic Voltammetry |
| DAC | Digital to Analog Converter |
| DL | Diffusion Layer |
| EIS | Electrochemical Impedance Spectroscopy |
| EPS | Electrode Potential Slope |
| LSV | Linear Sweep Voltammetry |
| MFC | Microbial Fuel Cell |
| MISO | Master In Slave Out |
| MOSI | Master Out Slave In |
| MUX | Multiplexer |
| NAD | Nicotinamide Adenine Dinucleotide |
| NADH | Nicotinamide Adenine Dinucleotide Hydrogene |
| NHE | Normal Hydrogene Electrode |
| OCP | Open Circuit Potential |
| OCV | Open Circuit Voltage |
| Op-amps | Operational Amplifiers |
| ORR | Oxygen Reduction Reaction |
| PCBs | Printed Circuit Boards |
| PEM | Proton Exchange Membrane |
| RE | Reference Electrode |
| SEA | Separator Electrode Assembly |
| SHE | Standard Hydrogene Electrode |
| SPA | Spaced Electrode Assembly |
| SPI | Serial Peripheral Interface |
| UMFC | Upflow Microbial Fuel Cell |

| | |
|-----|-----------------------------------|
| UWE | University of the West of England |
| VCE | Counter Electrode Voltage |
| WE | Working Electrode |

Chapter 1

1. Introduction

This first chapter briefly explains outlines the dissertation structure. It starts by presenting the motivation to develop this work, passing through the main objectives, and, finally, providing an overview of each chapter's contents.

1.1. Motivation

Nowadays, the field of renewable energies is in constant change. New technologies are emerging. The diversity of power sources is enormous—all of this to replace fossil fuels with renewable energies and provide a sustainable future to the planet. Microbial fuel cells are an example. Consequently, studying this type of cells was necessary to develop a dynamic interface to their monitorisation.

1.2. Main goals

The main aim of this dissertation is to understand how a MFC works and identify the quantities that describe its operating status. A potentiostat is a device that makes it possible to impose a potential and measure the current that result from that imposition. The present dissertation study the development of a potentiostat that allows studying the behaviour of a MFC. The development instrumentation should be used to carry out MFC studies with the aim of characterize them and understanding their functioning.

1.3. Outline

Apart from this first chapter in wich is introduced the work made and its motivations, the dissertation is structured as it follows.

Chapter 2 describes the concept, the working process, the structures, and application of the MFCs.

Chapter 3 explains how the potentiostat works by describing the functioning process and the necessary electronic circuits. Electrochemical analysis methodologies using the potentiostat to study the microbial fuel cells are also presented.

Chapter 4 uses the knowledge presented by the previous two, and provides a state of art about how to study MFCs using potentiostats.

Chapter 5 explains the potentiostat experimental setup. The circuit schematics is presented and discussed. The functions of the node-red interface, and the mbed code used to control the potentiostat operation and interface with the computer.

Chapter 6 is about the methodology that would be used to study the MFCs reactors and the reality of the simulation using dummy cells.

Finally, chapter 7, present the conclusions of the dissertation and the guidelines for future work.

Chapter 2

2. Microbial Fuel Cells

This chapter is relative to understanding the MFC concept, its importance, and the possibilities for its usage in the future.

2.1. Concept and evolution in the study of MFCs

MFCs use bacteria as catalysts to oxidise organic and inorganic matter and generate current. The electrons produced by the bacteria from the substrates are transferred to the anode, the negative terminal, and flow to the cathode, positive terminal, linked by a conductive material containing a resistor or operated under a load. By convention, a positive current flow from the positive to the negative terminal is opposite to that of electron flow [1].

Bioelectricity generation was first demonstrated approximately a century ago, while the MFC, as we know it, from recent work, needs to be considered a new technology. Many challenges need to be solved to fully exploit the maximum power production possible by MFCs, to find ways to make the systems economical [2].

The field application of MFC technology is restricted by its design aspects and technological, electrochemical, and microbiological limitations. MFCs are under deep research in almost all aspects of their operation, and several MFC configurations have been developed in close alignment with conventional electrochemical and fuel cell designs. However, considering the limitation of electrochemistry and charger transfer, the anodic chamber volume of MFCs is restricted. However, such structures cannot avoid the resistances created by scaling up the reactor. Transferring lab-scale to field-scale level and making MFCs competent with existing wastewater treatment processes with cost-effective design is a major challenge for MFC researchers. Therefore, it is essential to consider all physical, chemical, electrochemical, engineering, and microbial processes and their integration, when extrapolating to scaling up or conceptually different reactor architectural designs. [2]

MFCs are a promising technology for renewable energy production, and their most likely near-term applications are a solution for simultaneous wastewater treatment and electricity production. MFCs are useful in other specialised applications, as well as power sources for environmental sensors and bioremediation. With modifications, MFC technologies could find applications ranging from H₂ production to renewable energy production from agricultural biomass. The number of papers published by year related to MFCs' research is shown in the Figure 2.1. Since 2001 that this number has started to increase exponentially until today.

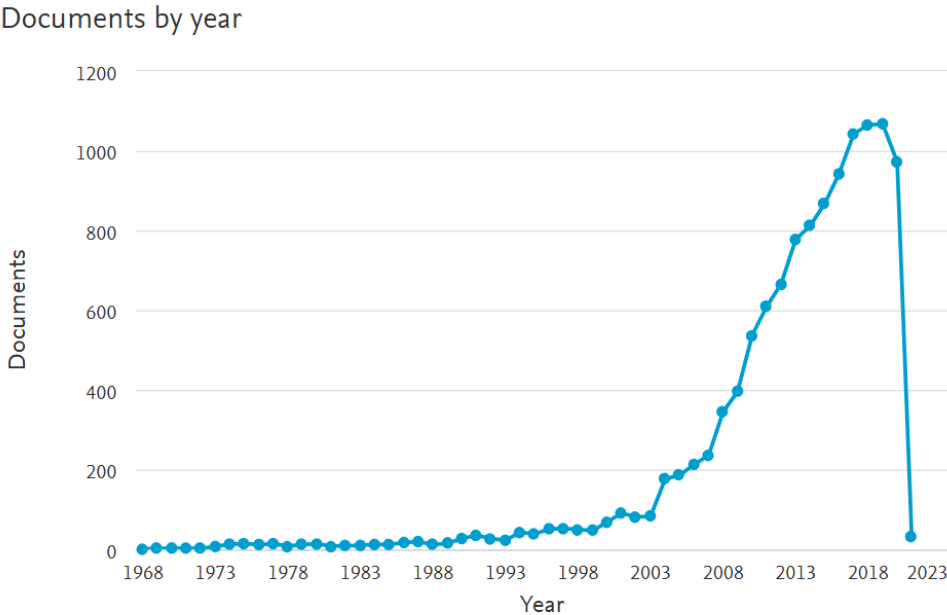


Figure 2.1: Evolution graphic of MFCs research. From [3].

Most early MFC studies were not conducted to optimise volumetric power density but rather to explore materials and understand factors that limited power on an area basis. As systems have been designed to improve performance based on reactor volume, power volumetric power densities have increased for MFCs using oxygen at the cathode. It is expected that these powers densities continue to grow in the next few years. The fundamental goal of an MFC design will be economically based on capital and operational costs compared to that needed for conventional designs. [2]

The curiosity about MFCs has been growing exponentially since the beginning of the 21st century. In the beginning of the last century, the English botanist Michael Potter wrote the first report about MFC, demonstrating that microorganisms could generate voltage and deliver current. Later in the 1960s, Biological fuel cells (BFCs) became popular when NASA showed short-term interest in turning organic waste into electricity on space

missions. After this, interest in the MFC functionalities raises, with a focus on mediator-based electron transfer. The number of publications and citations illustrates this interest. [4] A schematic about MFCs history through the years is shown in Figure 2.2.

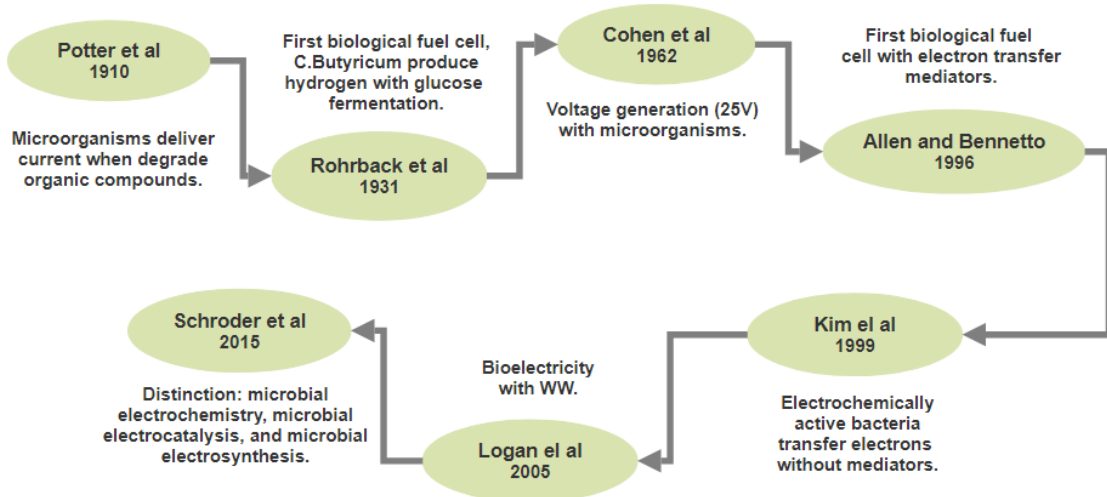


Figure 2.2: Schematic of MFCs history.

Ever since the conception of an MFC by Michael Potter in 1910, the technology has often had the reputation of a lab scientific curiosity rather than a helpful technology. This situation had both a positive and a negative impact on technology, becoming a scientific field. The positive effect is that numerous research groups use the MFC technology as a scientific tool for understanding microbial, biochemical, electrochemical and material surface reactions under controlled conditions and investigate how these can be influenced by choice of materials, feedstock substrates and chemical compounds. As a negative aspect, it is possible to highlight that MFC's technology isn't considered a serious contender in the wastewater treatment field or the renewable energy sector. It is perhaps the only example of a technology that can generate, rather than consume, energy from the cold oxidation of waste organic matter. There have been several reports of MFC implementation in various applications, precisely demonstrating the practical value of the technology. [4]

2.2. Biochemical process

Microorganisms degrade organic matter producing electrons, that go through various respiratory enzymes in the cell, and produce adenosine triphosphate (ATP) energy. Many electron acceptors such as oxygen, nitrate or sulfate diffuse into the cell where they accept electrons, forming products that can diffuse out of the cell. The electrons are later released to an electron acceptor that receives the electron and becomes reduced. It is also possible to transfer electrons to the outside the cell, exogenously transferring electrons. This process can also produce energy in an MFC.

The generation method allows understanding MFCs operation and classification. MFCs are classified about the method of generation of electrons as electrogenesis, the bacteria as exoeletrogens and the reactor. [2] The schematic system of the MFCs is shown in Figure 2.3.

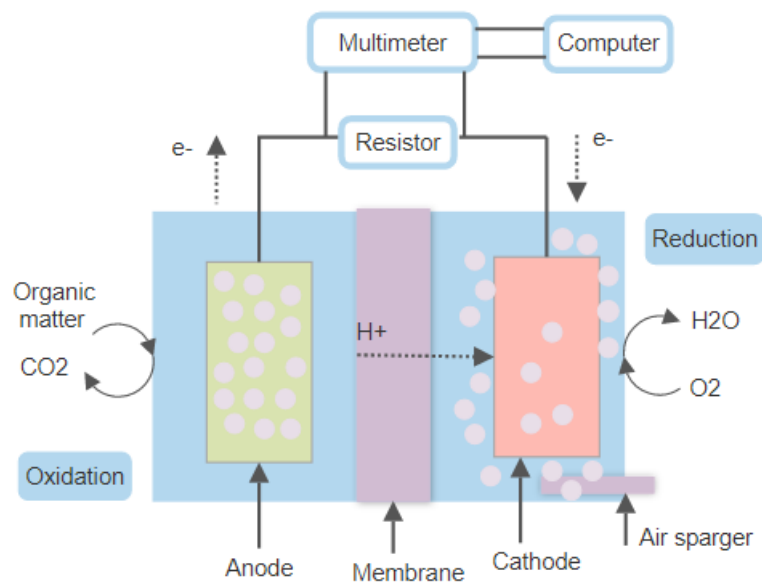


Figure 2.3: System of an MFC.

The inhibition of electricity generation is made in the anode chamber by oxygen. Therefore, the system must keep the bacteria separated from oxygen, usually by placing a membrane that allows charge transfer between the electrodes, creating two distinct chambers, the anode chamber where bacteria grow and the cathode chamber where the electrons react with the catholyte. The cathode is sparged with air to provide dissolved oxygen for the reaction. The two electrodes are connected by wire with a resistor. The membrane is permeable to protons produced at the anode so that they can migrate to the cathode, where they combine with the electrons transferred, via the wire and oxygen,

forming water. The current produced by an MFC is typically calculated in the laboratory by monitoring the voltage drop across the resistor using either a voltmeter, a multimeter or a potentiostat connected to a computer for essentially continuous data acquisition. [2]

Bacteria that evolved on the planet were likely able to use several different types of electron acceptors, but the most interesting for the MFCs were bacteria able to transfer electrons outside the cell. Exoelectrogenic bacteria are distinguished from the anaerobes that don't need oxygen to survive. Their ability to instantly transport electrons outside the cell permits them to function in an MFC.

Electrochemically active biofilms are essential in natural environments. Principally, in metal oxidation and reduction actions and the associated effects on mineral dissolution, the carbon cycle and the sorption and complexation of phosphorus and heavy metals. Besides this, they may have a significant role in fulfilling a need for bioenergy production through direct electricity generation.

In terms of the diversity of bacteria capable of exoelectrogenic activity, many discoveries have been made. An important one was that power could be produced with *E. coli* K12 HB101 in an air-cathode MFC when this bacterium was electrochemically evolved in fuel cell environments through natural selection. A suspension of the bacterium was prepared and loaded into an MFC. Samples from the reactor were re-cultivated. There was increased power output in this reactor without the need for the addition of mediators. This result suggests that *E. coli* can be evolved to exhibit electrogenic activity. [2]

As it was seen, bacteria grow by catalysing chemical reactions and harnessing and storing energy in the form of ATP. Some bacteria reduce the substrate by oxidation. Electrons are transferred to respiratory enzymes by nicotinamide adenine dinucleotide hydrogen (NADH), the reduced form of nicotinamide adenine dinucleotide (NAD). These electrons flow down a respiratory chain, a series of enzymes that function to move protons across an internal membrane, creating a proton gradient. The protons flow back into the cell through the enzyme ATPase, creating 1 ATP molecule from 1 adenosine diphosphate for every 3 or 4 protons. The electrons are finally released to a soluble terminal electron acceptor, such as nitrate, sulfate, or oxygen, as it was seen before. [5]

The maximum potential of the process is around 1.2 V. A cation-exchange membrane can also be used to separate the catholyte and the liquid in contact with the anode into different chambers, or just to act as a barrier that keeps chemicals and materials other

than protons from reaching the cathode. In the case shown in Figure 2.4, bacteria could derive energy from the potential between NADH and cytochrome c, which is a protein associated to mitochondria, whereas the MFC could be used to recover energy from the potential between cytochrome c and oxygen. Actual potential depends on the concentrations and potentials of specific enzymes and electron acceptors. [5]

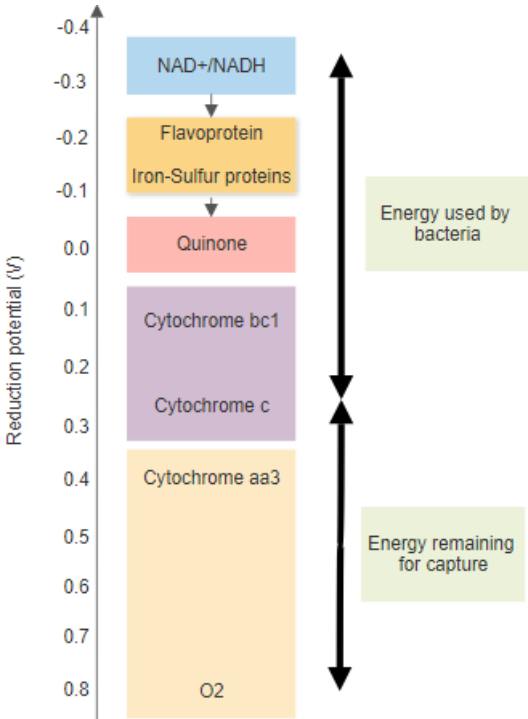


Figure 2.4: Biochemical example.

2.3. MFC components

There are many different configurations used for MFCs controlled by the performance efficiency of the individual component, electrochemical properties of electrode material, and the resistance posed by these components, which finally decides the overall internal resistance of the cell and its power output. The anode material and its configuration are an important parameter in an MFC, as it leads the growth of the microbial biofilm and facilitates electron transfer involved in the bioelectrochemical reactions. [6]

The anode material must be highly conductive, non-corrosive, high specific surface area per volume, high porosity, non-fouling which means that the bacteria do not fill it up, inexpensive, and easily made and scaled to larger sizes. Among these requirements the important to take is that the material must be electrically conductive. [2]

In an MFC, the water conducts the protons, therefore a membrane is not necessarily needed as a system component. The membrane is mainly used in two chambered MFCs as a method for keeping the anode and cathode liquids separate. The membranes must be permeable so that the protons produced at the anode can migrate to the cathode. They also serve as a barrier to the transfer of other species in the chamber. Even in single-chamber MFCs, membranes can be useful to isolate the catalyst from the cathode. Some disadvantages are their high cost and that they decrease system performance. The adverse effect of the membrane on performance is usually a result of increased internal resistance. If the solution conductance or effective diffusivity of a proton, or chemical species carrying a proton, is reduced by the presence of the membrane then the internal resistance of the system will increase, and the power production will be reduced.

Other component of MFC is the cathode, that represents one of the most crucial due to the chemical reaction that occurs there and it's difficult to engineer as the electrons, protons and oxygen must all meet at a catalyst in a tri-phase reaction, solid catalyst, air and water. The catalyst must be on a conductive surface, but it must be exposed to both water and air so that protons and electrons in these different phases can reach the same point. The materials used are mainly carbon paper, cloth, graphite woven graphite, graphite granules and brushes. The difference when these materials are used for the cathode is that a catalyst is usually but not always needed. Solid phase and liquid catalysts have been used, creating a wide range of possible materials and chemicals to facilitate current generation. The most used material for a cathode is carbon paper pre-

loaded with catalyst on one side. When used in the MFC, the side containing the catalyst faces the water, with the uncoated side facing air.

The choice of cathode material is also based on applications. In MFC a typical cathode setup has three layers, diffusion layer (DL), conducting support material, and catalyst. The cathodic reduction reaction plays an important role in enhancing the power generation from MFC. Materials for anode and cathode are in most situations the same, however, to achieve effective oxygen reduction reaction (ORR), it is necessary to coat it with a catalyst layer. [2]

Finally, two and three electrode configurations are commonly employed to determine MFC and electrode performances. A four-electrode configuration is sometimes used when the conductivity of an electrolyte, the membrane, or electrode material is tested by electrochemical impedance spectroscopy (EIS). In practice, a MFC only needs two electrodes for electricity generation, an anode, and a cathode.

A variety of materials have been used as electrodes: graphite foil, rods, granules, and fibre brush; carbon paper, cloth, felt, and foam; activated carbon cloth; reticulated vitreous carbon; electrodes modified with conductive polymers; and metals such as aluminium, nickel or stainless steel. [7]

2.4. Architectures

As it was seen, a large range of materials have been used in MFCs, but how they are arranged and used in the final system design, named as architectures, is what dictates how the system will perform in terms of power output, Coulombic efficiency, stability, and longevity.

There are the air-cathode MFCs, which exist in various formats. The cube reactors are a useful and simple design for examining what affect power production in MFC. The single-chamber, air cathode cube reactors have been the most used architecture of all the existent. It consists in single 4-cm block of acrylic or lexan drilled through producing a 3-cm diameter chamber. The empty bed volume is 28 mL and when the two electrodes are placed on opposite ends the surface are aper volume of the reactor is 25 m²/m³. Two openings are made on the top to allow the reactor to be easily drained and filled. These are sealed with thick stoppers to prevent oxygen from entering the reactor when he is operated. The electrodes sit in the ends that are cut to be slightly recessed, a round rubber gasket placed over the electrode, and then the flat plate ends are attached on top of the gasket to form a watertight seal. [2]

So, this single-compartment MFCs offer simpler and economic design. They are simple anodic chamber where there is no definitive cathode compartment. Porous cathodes formed on exterior side of the wall of the anodic chamber utilise oxygen from atmosphere for ORR using catalysts. These designs are easy to scale up and therefore extensively utilised for research with certain variety. [6]

Continuing the air-cathodes there are the two-chamber system. The 4-cm reactor with an air cathode was adapted to study the effect of different membrane on internal resistances. A membrane was placed into the middle of the reactor, creating two equally sized chambers, one where the bacteria and solution were placed, and the second containing just buffered solution. [2] In Figure 2.5 we can see the architecture of one and two chamber MFC reactor.

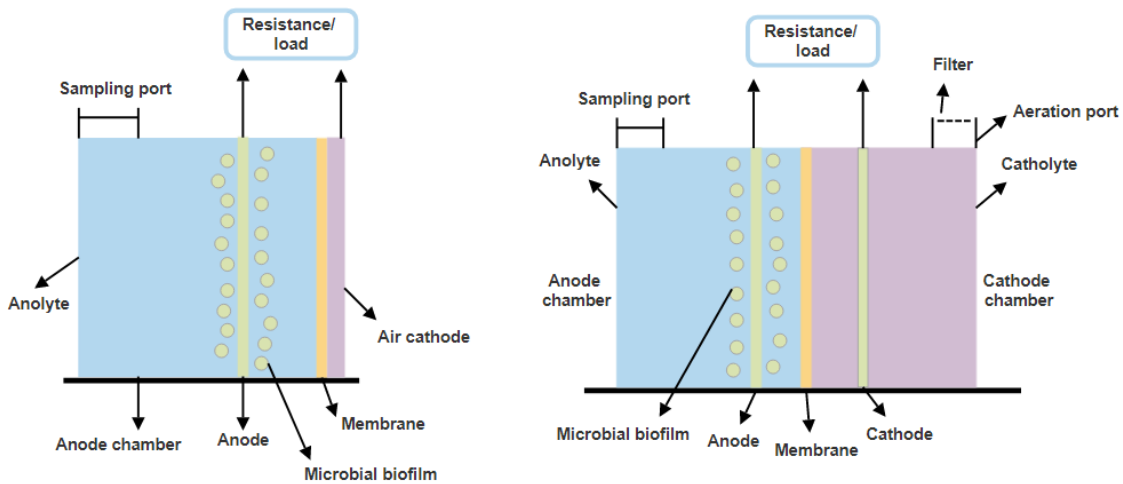


Figure 2.5: One chamber reactor (left) and Two chamber reactor (right).

With this changes, the two chamber MFC contains an anodic and a cathodic chamber separated by a proton exchange membrane, a separator, or a salt bridge to allow proton transportation to the cathode while restricting the diffusion of oxygen into the anode. The chambers can take various practical shapes for tailoring the architectural design such as tubular, hexagonal, rectangular, serpentine, or micro-MFC. [6]

More experimental work has been done with pure cultures necessitating a system which can be easily autoclaved and kept sterile. A bottle type of single-chamber, air cathode, was also developed and tested using pure and mixed cultures. The reactor consists of a standard laboratory bottle modified to contain a side arm, essentially one bottle of a two-chambered reactor, with a side arm of a larger diameter than typically used. [2]

In Figure 2.6 is presented the schematic, in evidence the anode where bacteria form a biofilm on the surface through a air sparger, and the cathode, exposed to dissolved oxygen. The two chambers are separated by a cation-exchange membrane (CEM), that ideallt allows the exchange of protons through the electrolyte and not through oxygen or the substracte. Also in Figure 2.6 is shown an example of a simple two-chamber system with the CEM clamped between the ends of two tubes, joined to each bottle. [5]

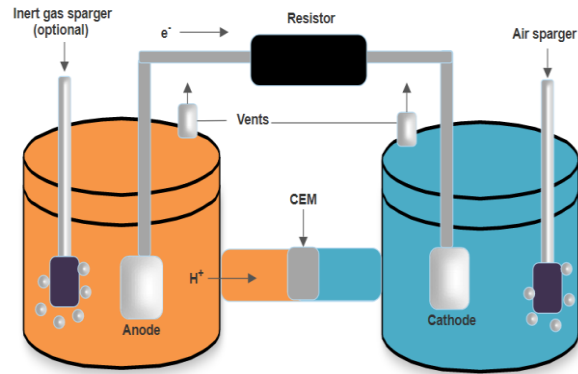


Figure 2.6: H-type MFC example

The MFCs with membranes are also studied, however, there are some inherent problems associated with membranes such as the high cost of the proton exchange membrane (PEM), if applied, biofouling, and high internal resistance. In the MFCs without membranes, often oxygen acts as the terminal electron acceptor. The elimination of membrane can simplify the MFC design and decrease the cost and the internal resistance. Various MFCs without membrane were developed and their configuration may be single or two chambered, but due to absence of membrane. [6]

Many others configurations have been designed and tested, such as aqueous cathodes using dissolved oxygen, two chamber with soluble catholytes such H type, tubular packed reactors, stacked MFCs or even upflow MFC (UMFC), as it is presented in Figure 2.7.

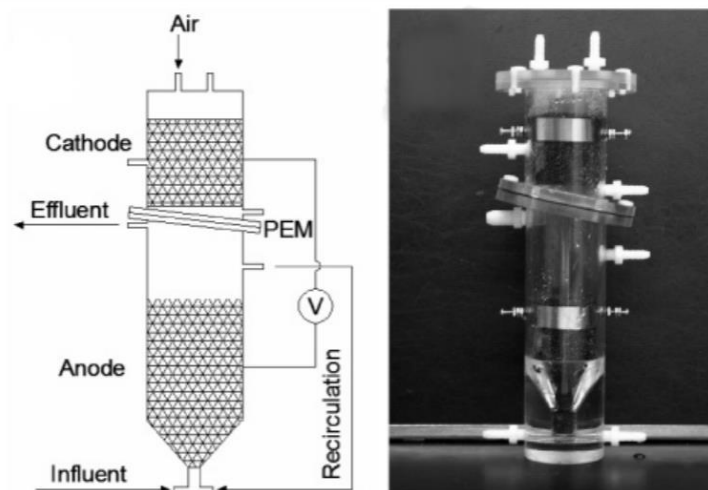


Figure 2.7: Schematic and picture of UMFC (adapted from [33])

2.5. Applications

The most known application of MFCs is wastewater treatment but exists other examples. Renewable energy production is a longer-term prospect that requires substantial technical and manufacturing advances from more near-term applications. [5]

In terms of wastewater treatment, a system based on MFC gives a great opportunity to develop the technology, because the substrate is free, and wastewater has to be treated. The major problems on this application are the scale-up and material issues. An MFC system could even be useful for individual homes or other small applications, although power production would probably be too low to warrant recovery of electricity. Septic tanks are typically used for single to multiple house applications, but they are inefficient systems for removing Biochemical Oxygen Demand (BOD) or nutrients. MFC applications may be particularly useful in areas where septic tanks cannot be used because of the need for high BOD removal. Such applications are currently carried out by small aerobic systems that consume energy, often in remote areas with little power available to run them. [8]

Environmental sensors are also a possible application. Data on the natural environment can clarify and modelling ecosystems responses, but sensors distributed in the natural environment require power for operation. MFC can possibly be used to power such devices, particularly in river and deep-water environments where it's difficult to routinely access the system to replace batteries. [8], [9]

The first example of a microbial metabolism working in a practical application, such as bacterial-robots, is the 3-wagon toy train, which employed an artificial stomach filled with *E. coli* metabolising sugar, the reduced chemicals from which were fed into a stack of chemical fuel cells, which produced energy to charge the bank of Ni-Cd batteries that were powering the train's motors and pumps. Two years later, EcoBot-I was reported as the first robot which was directly powered by MFCs fed with glucose without using batteries, solar cells or any other form of conventional power source. EcoBot-I employed electrolytic capacitors for temporarily storing the energy from the MFCs aboard, and once full, the energy was released to actuate the locomotion motors and move towards the light. Later, EcoBot-II was reported as the next generation in the family of EcoBots, which in addition to being phototactic, was also able to report temperature wirelessly, without being dependent on chemical mediator, unlike the first two robots. These early examples showed that it is possible to have artificial agents powered by microbial

metabolism inside MFCs but did not demonstrate the essential element of self-sustainability, since human intervention was still required to either replenish or replace chemicals and feed the MFCs. [4]

The first example of a self-sustainable robot that had its own circulatory system and was able to complete the thermodynamic cycle of ingestion-digestion-egestion was EcoBot-III. This robot demonstrated autonomy and simultaneously showed that miniaturising the MFCs and multiplying the units into a stack, is one viable approach to scaling up the technology. After this robot, there was a few releases with some improvements. To show that, is in Figure 2.8 a scheme of the chronological order of the robots.

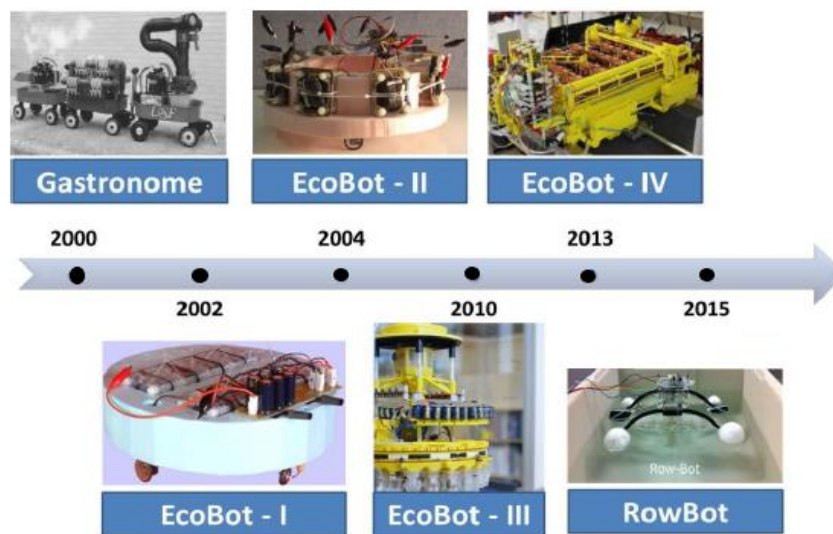


Figure 2.8: Chronologic order of the MFC powered autonomous robots (adapted from [10])

The first demonstration of MFCs doubling up as biological oxygen demand sensors predates the Gastrobot and EcoBot development and this revealed the unique advantage of the technology to operate as a remote sensor. Benthic MFCs had also been subsequently reported for powering a meteorological buoy, presented in Figure 2.9, wireless temperature sensors and other conventional environmental sensors. [4]

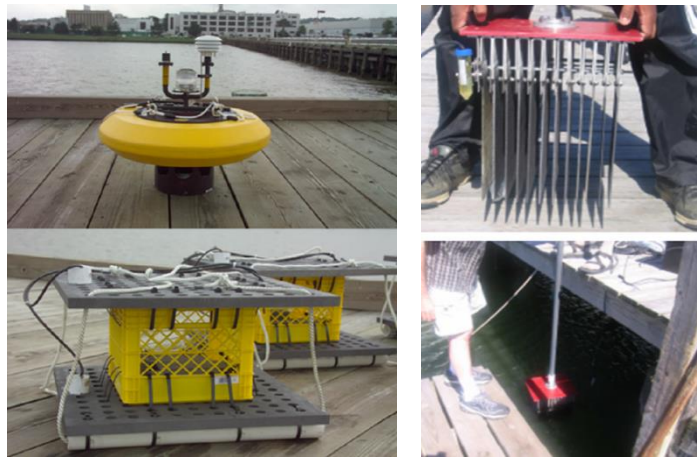


Figure 2.9: Meteorological buoy powered by MFCs (from [34])

Several other applications have been reported including the first demonstration of a self-sustainable MFC stack, with sufficient energy to power its own feeding and hydration pumps and sustain long-term operation; the powering of a Texas Instruments Chronos digital wristwatch; the charging of a basic mobile phone and a smartphone and LEDs for internal lighting. This application has led to the Pee Power urinals, which are being developed for trialing in refugee camps and slums. [4]

A basic mobile phone charged by a stack of 12 ceramic microbial fuel cells, and the Pee Power urinal were tested on the University of the West of England (UWE), as is shown in Figure 2.10. Although these may still be considered as proof-of-concept exemplars, they are nevertheless showing that the MFC technology can have multiple applications, at multiple scales in multiple environments, by allowing the constituent microbes to do what they naturally do biotransform organic matter. [4], [11]



Figure 2.10: Pee power urinal at UWE campus in 2015 (from [11])

Chapter 3

3. Potentiostat

This chapter presents the potentiostat, its fundamentals, the electronic behind of his function, the possible electrochemical analysis and in the end some applications of the low cost version.

3.1. Characteristics

Potentiostats are amplifiers used to control a voltage between two electrodes, a working electrode (WE), and a reference electrode (RE), to a constant value. To know that RE are electrodes, which maintain a constant voltage referred to the potential of the hydrogen electrode. A silver wire, covered with a silver chloride layer, dipping in a chloride solution, is a simple RE. To maintain a constant potential difference between the RE and the WE it is introduced a third electrode, the counter electrode (CE), as it is shown at the Figure 3.1. [12]

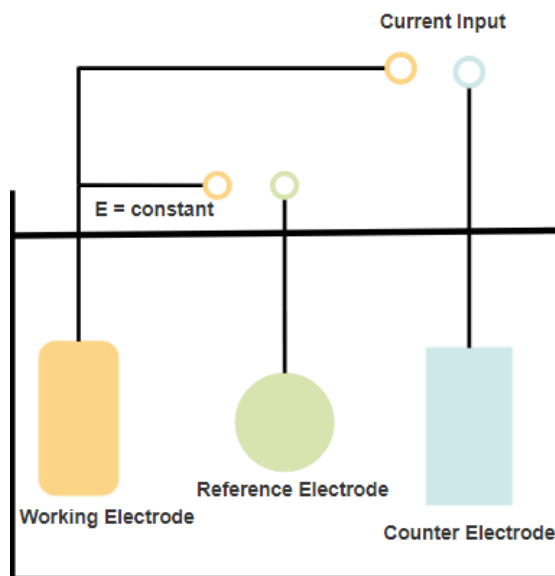


Figure 3.1: Basic potentiostat scheme

A current is forced between WE and CE, high enough and in proper polarity to keep the WE potential at a constant value with respect to the RE. There are many characteristics that can be associated to the potentiostat, such as control speed, accuracy, current range and dynamics, noise, stability and finally phase correction. In control speed, the

potentiostat must be able to react at appropriate speed of the chemical reaction. In terms of accuracy, the potentiostat counterbalances voltage difference between set control voltage and existing cell potential only to a good approximation. Residual errors remain, but the total error has other and more influencing sources such as uncompensated cell cable resistances and resistance effects in the cell. [12]

In a potentiostat, the most sensitive circuit is the input stage, producing noise in the input resistor and the first amplifier stage. A good potentiostat is equipped with low-noise amplifiers. However low-noise operational amplifiers (Op-amps) usually do not possess high input resistivity, or they have a restricted frequency range. It is essential to choose the input stage amplifier according to the main purpose of the potentiostat. A potentiostat used for a wide variety of electrochemical tests must show good stability, as the electrodes act in the control circuit, with all their variety of capacities, resistances, and frequency dependent impedances. Connecting a dummy cell with pure ohmic load, current and potential should be in phase as near to the theoretic limits as possible. Otherwise, certain experiments like measurement of impedance, produce wrong results.

The potentiostat, produces extreme low noise and controls currents from femtoamperes to kiloamperes. If it is very fast, its usual a certain amount of noise. To reach a high power potentiostat, there is no point to measure extreme small currents with it. But within the limits, potentiostats are versatile instruments. So, the advantages of potentiostat are that he is fast and low noise, and that the drawbacks are floating current measurement only, no output for the measurement of the existing potential. [12]

A flow diagram for potentiostat control system is presented in the Figure 3.2. The microcontroller uses the timer-capture module to provide interrupts at periodic intervals, since the periodicity of these interrupts determines scan rate. During an interrupt, the 10-bit up-down converter values are updated, the Analog/Digital measurements are taken, and the serial Digital/Analog contents are updated. [13]

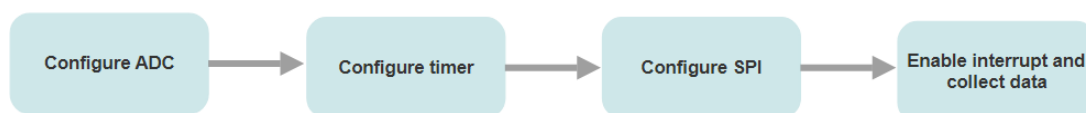


Figure 3.2: Potentiostat control system.

3.2. Circuit

Is described in [13] the implementation of a low cost potentiostat with Op-amps and the corresponding circuit is in the Figure 3.3. The input triangular-voltage waveform is fed to a current buffer, Op-amp A, and to the RE. In a current buffer, the input is isolated from the output and, thus, the current at the output of the Op-amp is not limited by input current and can provide infinite current. This satisfies the basic requirement for a CE, which needs to be able to provide any amount of current required by the electrochemical activity at the WE. The electrochemical current generated at the working electrode is converted into an equivalent voltage by Op-amp C, which is a current to voltage converter and can be measured using an oscilloscope or microcontroller circuitry. The RE is tied to the input of Op-amp B, which has infinite input resistance, in the range of Mega ohms, and hence there is very little current through the RE.

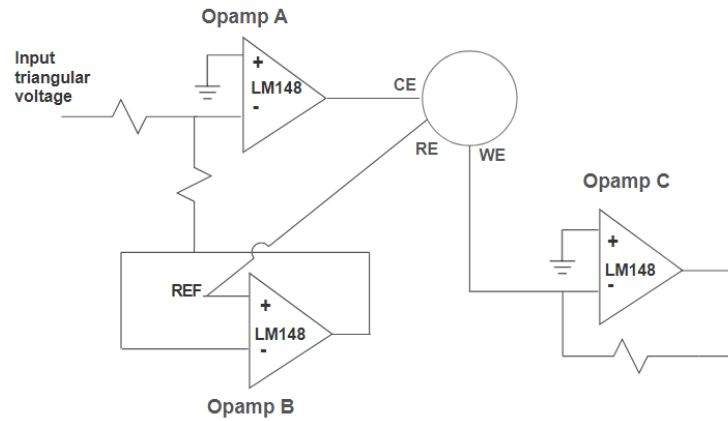


Figure 3.3: Potentiostat circuit.

Input to the potentiostat circuit can be provided through a laboratory waveform generator and the output can be monitored using an oscilloscope. Alternately, a microcontroller can be used to control the potentiostat circuit. [13] A basic circuit schematic of a microcontroller-controlled potentiostat is presented in Figure 3.4.

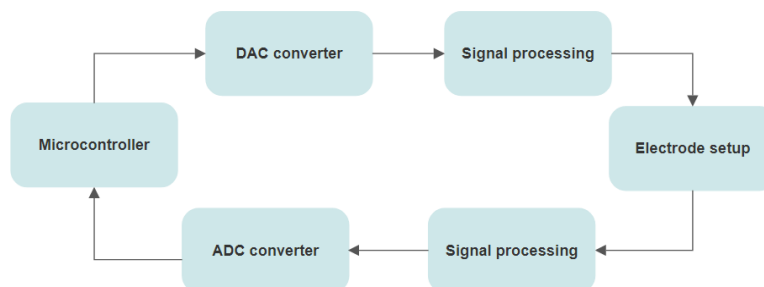


Figure 3.4: Microcontroller controlled potentiostat.

3.3. Electrochemical analysis

A more detailed understanding of a bioelectrochemical system can be obtained using a potentiostat. In MFC experiments, the potentiostatic mode of this instrument is often used for voltammetry tests in which the potential of the WE is varied at a certain scan rate, expressed in V/s^{-1} . In the case where a scan only goes in one direction, and the signal is a linear voltage ramp, the method is referred to as linear sweep voltammetry (LSV), if the scan is also continued in the reverse direction and comes back to the start potential, in a triangular shape, the method is cyclic voltammetry (CV). Other very often used electrochemical experiment is called chronoamperometry where a constant voltage signal is applied, and the current is measured over time. [1]

Voltammetry can be used for evaluating the electrochemical activity of microbial strains, determining the standard redox potentials of redox active components, and testing the performance of the cathode materials. A potentiostat can also be operated in a two-electrode setup to obtain polarisation curves or to determine the ohmic resistance using the current interrupt technique. In the two-electrode setup, the WE connector is connected to the cathode, positive terminal, and both the CE and RE connectors are connected to the anode.

More advanced measurements can be made when the potentiostat is equipped with a frequency response analyzer, allowing EIS. In EIS a sinusoidal signal with small amplitude is superimposed on the applied potential of the WE. By varying the frequency of the sinusoidal signal over a wide range and plotting the measured electrode impedance, more information can be obtained about the electrochemical system, such as the ohmic and internal resistance of an MFC, as well as to provide additional insight into the operation of an MFC. [1]

Cyclic voltammetry

The most common technique to determine the mechanisms of electrode reactions is CV, which requires a three-electrode configuration to obtain accurate results. MFC studies employing this technique generally use forward and backward voltage sweeps with rates in the range of $1-100\text{ mV/s}^{-1}$. CV experiments have been used extensively to investigate the mechanisms of electrode reactions involving both direct and indirect electron transfer between the biofilm and the electrode. It is also possible to determine the redox

potentials of the chemical or biological species involved at the anode or cathode. Finally, it can be evaluated the performance of the catalysts being studied. [7]

In order to explain this technique, there are some concepts to take in consideration, such as redox potentials, the polarization curve, the voltammogram, the peaks and also the scan rate.

The redox potential values of different substances are known, their presence in a liquid can easily be demonstrated. This is done by gradually increasing or decreasing the potential using a potentiostat. Such tests are often carried out in electrochemical research. If the potential is gradually increased from a point below the redox potential, a reductive electron current is measured, which will become smaller until the redox potential is reached. After that point an oxidative current will occur and grow larger, as the potential is further increased. This development can be seen in a voltammogram. [14]

A voltammogram is a graphic that can be achieved after an electrochemical experiment. It has a typical form in which the electron flow, current, is measured against the potential. The typical shape of the voltammogram is relative to the way in which an electrochemical experiment is set up. There are two groups of measurements that are plotted as voltammograms, pulsed techniques and linear sweeps. [14]

The x-axis represents a parameter that is imposed on the system, the applied potential (E), while the y-axis is the response, the resulting current (i) passed. A crucial parameter is that $v = 100 \text{ mV/s}$. This value is called the scan rate (v). It indicates that during the experiment the potential was varied linearly at the speed, scan rate, of 100 mV per second. To illustrate this, in presented in Figure 3.5 an example of voltammogram. [14]

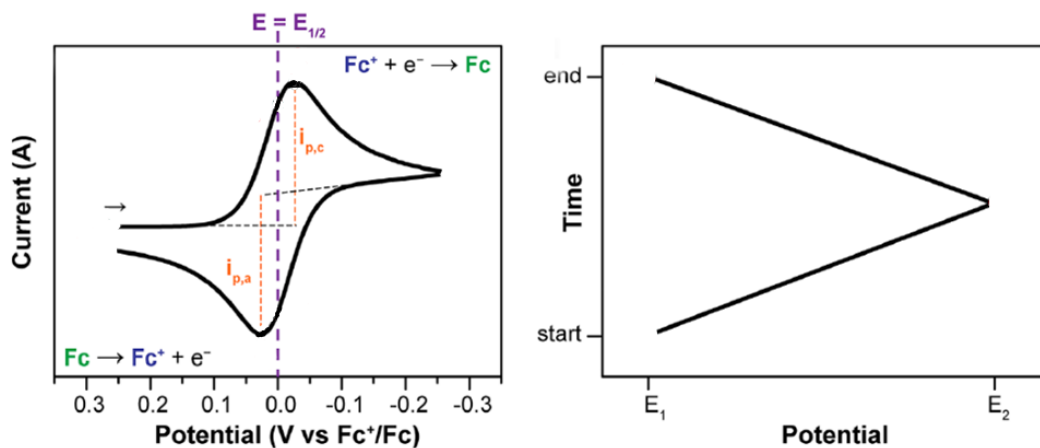


Figure 3.5: Voltammogram example (adapted from [14]).

In the right graphic is shown the relationship between time and applied potential, with the potential axis as the x-axis to see the relation with the corresponding voltammogram in left graphic. In this example, in the forward scan, the potential is swept negatively from the starting potential E_1 to the switching potential E_2 . This is referred to as the cathodic trace. The scan direction is then reversed, and the potential is swept positively back to E_1 , referred to as the anodic trace. [14]

There is an equation that provides a powerful way to predict how a system will respond to a change of concentration of species in solution or a change in the electrode potential. When the potential is scanned during the CV experiment, the concentration of the species in solution near the electrode changes over time in accordance with the Nernst equation. This equation relates the potential of an electrochemical cell, E , to the standard potential of a species (E^0) and the relative activities of the oxidized (Ox) and reduced (Red) analyte in the system at equilibrium. In Equation (3.1), F is Faraday's constant, R is the universal gas constant, n is the number of electrons, and T is the temperature.

$$E = E^0 + \frac{RT}{nF} \ln \frac{(Ox)}{(Red)} = E^0 + 2.3026 \frac{RT}{nF} \log_{10} \frac{(Ox)}{(Red)} \quad (3.1)$$

The scan rate of the experiment controls how fast the applied potential is scanned. Faster scan rates lead to a decrease in the size of the diffusion layer. Consequently, higher currents are observed. [14]

For electrochemically reversible electron transfer processes involving diffusing redox species, the Randles–Sevcik equation, in Equation (3.2) describes how the peak current i_p (A) increases linearly with the square root of the scan rate v ($V s^{-1}$), where n is the number of electrons transferred in the redox event, A (cm^2) is the electrode surface area usually treated as the geometric surface area, D_o ($cm^2 s^{-1}$) is the diffusion coefficient of the oxidized analyte, and C^0 ($mol cm^{-3}$) is the bulk concentration of the analyte.

$$i_p = 0.446nFAC^0 \left(\frac{nFvD_o}{RT} \right)^{1/2} \quad (3.2)$$

This equation can also provide indications as to whether an analyte is freely diffusing in solution. As analytes can sometimes adsorb to the electrode surface, it is essential to assess whether an analyte remains homogeneous in solution prior to analysing its reactivity. In addition to verifying that the analyte is freely diffusing, the Randles–Sevcik equation may be used to calculate diffusion coefficients. [14]

Linear Sweep Voltammetry

In LSV a fixed potential range is employed much like potential step measurements. However, in LSV the voltage is scanned from a lower limit to an upper limit. The voltage scan rate is calculated from the slope of the line. By changing the time taken to sweep the range we alter the scan rate. [15]

The characteristics of a linear sweep voltammogram recorded depend on several factors, including the rate of the electron transfer reactions, chemical reactivity of the electroactive species and voltage scan rate. In LSV measurements, the current response is plotted as a function of voltage rather than time, unlike potential step measurements. CV is very similar to LSV. To show the differences, it is illustrated in Figure 3.6 the typical voltammograms for each technique and presenting the critical parameters, which are the peak potentials E_p and the peak currents i_p . Also, there can be more than one peak in a cyclic voltammogram, and an additional subscript is used, being a to anodic and c to cathodic. [15]

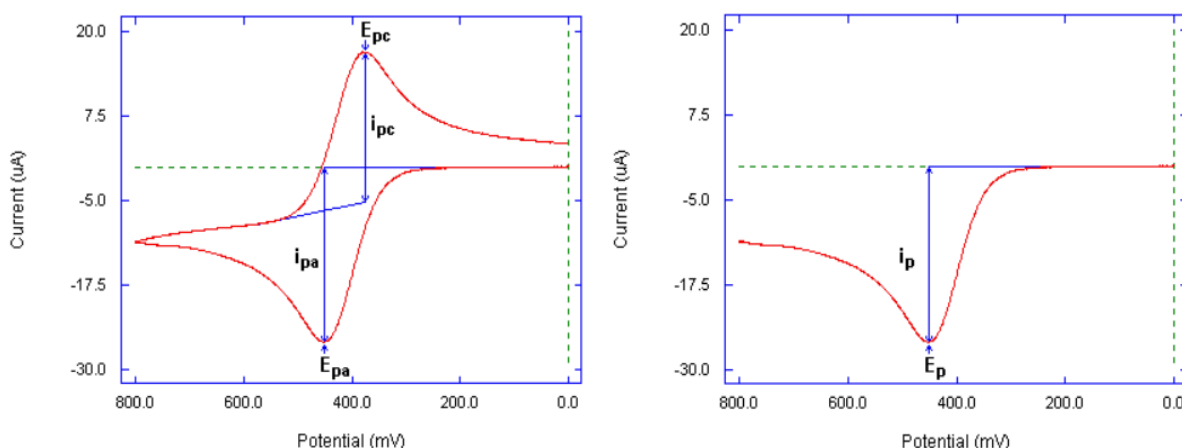


Figure 3.6: Typical voltammograms for CV (left) and LSV (right) (adapted from [15]).

Electrochemical Impedance Spectroscopy

EIS is one of the most complex techniques in electrochemical research. EIS allows separating the influences of different components that means the contribution of the electron transfer resistance, double layer, or capacity. As a result, EIS is interesting for analytical electrochemistry, because molecules can be detected without a redox active marker. This technique is also very surface sensitive, making many changes visible that other techniques don't see, for example, changes in polymer layers due to swelling,

surface changes due to protein adsorption or penetration of corrosion protection layers. The most popular plots for impedance spectra are the Bode plot and Nyquist plot, an example is shown in Figure 3.7.

A potentiostat measures the impedance by applying a potential wave to the working electrode and records the resulting current wave. From these two waves, the potentiostat calculates Z , Φ , Z' and Z'' . The spectrum is made by measuring these parameters for potential waves with different frequencies. [15]

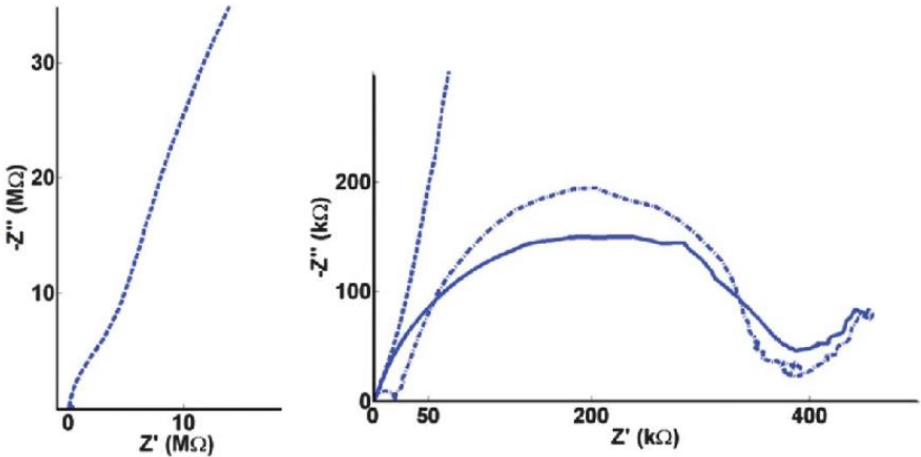


Figure 3.7: Nyquist EIS example (adapted from [15]).

3.4. Applications

The applications of potentiostats are numerous, being possible classification from traditional to low-cost potentiostats. Starting with the conventional potentiostats, they have the main application in chemistry laboratories with research objectives. They can measure the current signal through the electrodes while applying a static electric potential, which can provide insight into surface chemistry, reaction rates, and chemical concentrations.

A distinct field, from the mentioned one, uses the potentiostat in the recycling of batteries, as is shown in [16]. It exists a problem about the toxicity of cadmium that has still not been completely resolved. Till today, there have been several processes available for the recycling or recovery of spent Ni–Cd, nickel–metalhydride, and lithium-ion batteries. Have been made studies about the preparation process for thin Cu/Ni multi-layers by the galvanostatic and potentiostatic pulse electrodeposition techniques. This work aimed to develop an electrochemical technique for the separation and recovery of Cd and Ni metals from spent Ni–Cd batteries. The Cd recovery process is performed by means of a potentiostatic electrodeposition technique in a leach electrolyte that contains sodium citrate. The Ni element is recovered from the resulting solution by treatment with NaOH to precipitate Ni (OH)₂ fine powders. The recovery of Ni from leach liquor is approximately 97%, and Cd recovery is between 70-90%.

By the end of the 2000s, were made improvements in embedded devices as well as increased research demands that made academics to develop custom low-cost instrumentation for analytical experiments. The laboratory benchtop potentiostats are very expensive with cost upwards of \$10,000 with the particularity that only can be used in laboratory settings. Because of these factors, throughout the 2010s researchers have made several attempts to design handheld potentiostat which compromise on such unnecessary features while providing a significant level of portability and accuracy. The applications of this low-cost potentiostats have three main areas in terms of applications such as environment and chemistry, engineer, and education.

Firstly, one of the first applications for low-cost potentiostats, was presented in [9] the monitoring of biogeochemical processes in arctic peat soils. For this application, environmental and electrical engineering researchers designed a chronoamperometry enabled potentiostat that could work at harsh and freezing temperatures. Taking advantage of the redox reaction induced by bacterial respiration, it was possible to

monitor bacterial metabolism at the WEs continuously. Since there are many concerns in the impact of climate change on arctic ecosystems, the development of this potentiostat allow to characterise ecological phenomena that would not be possible to achieve by a benchtop potentiostat. The potentiostat is in Figure 3.8.



Figure 3.8: Photo of the potentiostat in the field (from [9]).

In a similar field, in [17], the low-cost "Ecostat" potentiostat is demonstrated to characterise environmental water samples in Figure 3.9. The goal is to avoid custom interfacing and controlling software commonly used by benchtop potentiostats. These circuits rely on clock signals, which means possibly noise in the frequency spectrum. So, to prevent this, it was fabricated two printed circuit boards (PCBs) and implemented a digital PI controller to improve the accuracy of the transimpedance amplifier. Besides that, isolating the analogue circuits reduced noise from the digital circuitry. The solution uses an ATmega328 microcontroller, demonstrating a significant improvement over "Cheapstat", a similar potentiostat from 2011. This device performs electrochemical measurements in the field with a fraction of the cost for a laboratory potentiostat.



Figure 3.9: Ecostat potentiostat (from [17]).

Other low-cost potentiostats for biosensors application in the field are available. An example is a device developed in 2018, a potentiostat that measures blood alcohol concentration, described in [18], that uses a three-electrode control scheme, and is able

to measure a 40 μL blood sample via chronoamperometry to achieve a current measurement sensitivity of 36 nA/ (g Ethanol/L of blood). The device can characterise blood alcohol content with the same accuracy as breathalyser, using a calcium alginate hydrogel, containing alcohol oxidase and horseradish peroxidase. So it can be an alternative for police use. The sample container and printed circuit board are almost the size of a coin and can interface with a smartphone to provide real-time measurements via their designed Lab-on-a-chip. It just needed a micro-USB port to acquire and load the chip's readings directly. This system is represented in Figure 3.10.

In terms of wireless, wearable electrochemical sensors, a device for real-time biometric monitoring was also developed, as is shown in [19]. It is a three-electrode low-cost potentiostat developed to characterise lactate concentrations. It is predicted future improvements to simultaneously make measurements of pH, sodium, and lactate from sweat during physical exercise.

Finally, another interesting application field is science education. An example from 2018 designated by "JUAMI" described in [20] shows a potentiostat compatible with LabVIEW. The graphical user interface performs CV, LSV, and chronoamperometry. The device has a relatively poor measurement sensitivity of 10 μA , but is significantly cheap. The implementation aim was high school or college usage to teach students about electroanalytical principles. The device is shown in Figure 3.10.

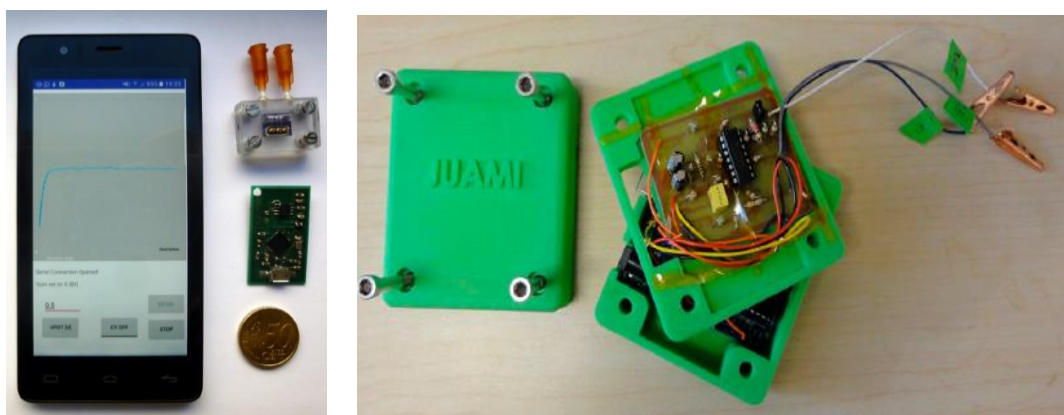


Figure 3.10: Blood alcohol system (left, from [18]) and JUAMI device (right, from [20]).

Chapter 4

4. Study MFCs with a low-cost potentiostat

Chemical measurements in microbial systems use conventional instruments, such as determining substrate concentrations and degradation products. The case of MFC experiments requires specialised electrochemical instrumentation. In most cases, cell voltages and electrode potentials measurement with commonly available multimeters is enough. Data acquisition systems are also simultaneously connected in parallel with the circuit.

Cell voltages are measured directly from the voltage difference between the anode and cathode. Electrode potentials use the RE included in the electrode compartment as a reference. Current determination from Ohm's law uses the measured voltage. The potentiostat provides a more detailed understanding of a bioelectrochemical system. The potentiostat controls either the potential or the current of an electrode. Obtained data is used to study the electrochemical response of the electrode at that specific condition. [1]

4.1. Study parameters

4.1.1. Electrode potential

The electrode potential is the starting point in the study of MFC's parameters using a potentiostat. Knowing the electrode potential requires the measurement of a voltage against an electrode with a known potential, such as a RE. This electrode contains several phases of constant composition and therefore has a constant potential. [1]

The standard hydrogen electrode (SHE), or normal hydrogen electrode (NHE), consists of a platinum electrode in a hydrogen saturated acidic solution with a potential of 0V. But since the NHE is not a practical reference electrode to work within an experimental setup, it is used a popular one, the silver/silver chloride (Ag/AgCl) RE, because of its simplicity, stability, and nontoxicity.

Electrode potentials are often dependent on the pH in the system, and it is, therefore, essential to report the solution pH. Usually, electrode potentials are reported in the literature calculated against the NHE, expressed in V or V vs NHE, or against the RE that

was used in the study (V vs Ag/AgCl). Because of these different methods, the electrodes' potential varies depending on the electrode used, the pH, and the cathode concentration of the electron acceptor. [1]

4.1.2. Power output

Another parameter that allows the evaluation of the overall performance of an MFC is power output. Power is calculated by Equation (4.1).

$$P = IE_{MFC} \quad (4.1)$$

Being E_{MFC} the measured voltage across a fixed external resistor, the current is calculated from Ohm's law, such as $I = E_{MFC} / R_{ext}$. Knowing this, it's possible to calculate the power output by Equation (4.2),

$$P = \frac{E_{MFC}^2}{R_{ext}} \quad (4.2)$$

This is the direct measure of electric power. The maximum power is calculated from the polarisation curve. [1]

4.1.3. Power density

It is known that the power output is usually standardised to the projected anode surface area because the anode is where the biological reaction occurs. The power density is calculated based on the area of the anode through Equation (4.3), where P_{An} is power density, in W/m², and A_{An} is the area of the anode,

$$P_{An} = \frac{E_{cell}^2}{A_{An}R_{ext}} \quad (4.3)$$

In many instances, however, the cathode reaction is thought to limit overall power generation. The anode consists of a material that can be difficult to express in terms of surface area. In such cases, the area of the cathode can alternatively be used to obtain a power density. [1]

Firstly, the voltage should be continuously measured and recorded, using a data logger against an applied external load of 100 to 1000 Ohms resistor. Once it is observed that voltage has steadied and had a similar value for few hours, then its possible to do

polarisation studies. For it must be connected the MFC to a resistor ranging from 10 Ohms to 20.000 Ohms. Then the output voltage of the MFC for each applied resistance must be measured. Using the resistance R and the voltage V with the Ohms law ($I = V/R$) is possible to calculate the current and the power, using $P = V \cdot I$. Power density and current density are obtained dividing these values by the surface area of the electrode. A simple example is, to an obtained power of 50mW, with an electrode surface area of 5 cm², the power density will be $50/5 = 10 \text{ mW/cm}^2$. [2]

To perform engineering calculations for size and costing of reactors, and as a useful comparison to chemical fuel cells, the power is normalised to the reactor volume where P_v is the volumetric power (W/m³), and v is the total reactor volume, the empty bed volume, as it is obtained by Equation (4.4). [1]

$$P_v = \frac{E_{cell}^2}{vR_{ext}} \quad (4.4)$$

4.1.4. Ohmic resistance

The ohmic resistance of an MFC can be determined using the current interrupt technique by operating the MFC in a current at which no concentration losses occur. Next, the electrical circuit is opened, resulting in zero current or infinite resistance. A steep initial potential rise is observed, followed by a slower further increase of the potential to the open-circuit voltage (OCV). The determination of the steep potential rise after current interrupting requires the fastest possible recording of the potential. Ohmic losses are proportional to the produced current and the ohmic resistance. When the current is interrupted, the ohmic losses instantaneously disappears. This result in a steep potential rise, E_R , in potential that is proportional to the ohmic resistance, and the current produced before the interruption. Using Ohm's law, obtained by Equation (4.5). The slower further increase of the potential to the OCV after the initial steep potential rise gives the electrode overpotentials that occurred during the current generation. [1]

$$R_{\Omega} = \frac{E_R}{I} \quad (4.5)$$

4.1.5. Polarisation curves

In this case of studying MFCs, polarisation curves are a powerful tool for analysing and characterising these fuel cells, representing the voltage as a function of the current density. Using the potentiostat polarisation curves can be recorded for the anode, the cathode, or the whole MFC, using an appropriate scan rate such as 1 mV s⁻¹. [1]

The polarisation curve should be recorded both up and down, from high to low external resistance, and vice versa. When a variable external resistance is used to obtain the polarisation curve, the current and potential values need to be taken only when pseudo-steady-state conditions have been established, and this event can take several minutes depending on the system. The reason for being temporary is that the substrate concentration in the reactor will change over long periods of time due to substrate demand at the anode. This will, in turn, affects the incidence of substrate products mass transfer over-voltage and current. Long-term recording may risk shifts in the microbial community. [1]

Besides this, polarisation curves can be divided into three zones. Starting from OCV at zero current, there is an initial steep decrease of the voltage, where the activation losses are dominant. Secondly, the voltage falls more slowly, the voltage drop is linear with the current, and the ohmic losses are prevalent. Finally, there is a rapid voltage fall at higher currents and the concentration losses, or mass transport effects, are dominant.

In MFCs, linear polarisation curves are most often faced. For this curve, the value of the internal resistance of the MFC is easily obtained from the polarization curve as it is equal to the slope, by Equation (4.6). [1]

$$R_{int} = \frac{-\Delta E}{\Delta I} \quad (4.6)$$

Power curve

The polarisation curve can calculate other important parameters, such as the power curve, that describes the power or power density as the function of the current or current density. [1]

In Figure 4.1, the right graphic is a power curve, based on the left graphic, that is polarisation curve. The effect of increased ohmic resistance on the shape of a polarisation

curve is shown on the left graphic from Figure 4.1. The solid curve is the original data set, while the dashed curve was calculated by including and additional ohmic resistance by subtracting a potential drop of $\Delta E_{IR} = I\Delta R_{\Omega}$.

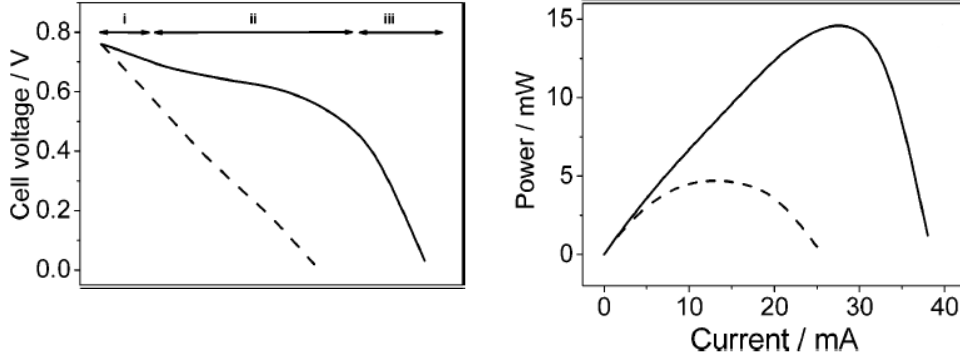


Figure 4.1: Polarization curve (left) and Power Curve (right) (adapted from [1]).

Increasing the ohmic resistance by this amount produces a linear polarisation curve (Figure 4.1, left graphic, dashed line), which is typically observed for MFCs. When a polarization curve is linear, the slope is equal to the internal resistance, as it is calculated by Equation (4.7).

$$E_{MFC} = OCV - IR_{int} \quad (4.7)$$

If the polarisation curve is not linear, the solid line, a current independent R_{int} cannot be defined and the system is better expressed in term of ohmic resistance R_{Ω} and the electrode overpotentials, which can be determined using the current interrupt method or EIS. In general, the difference between the measured cell voltage and the cell emf is referred to as overvoltage and is the sum of the overpotentials of the anode and the cathode, and the ohmic loss of the system. In Equation (4.8) the $\sum \eta_a$ and $|\sum \eta_c|$ are the overpotentials of the anode and the cathode respectively, and IR_{Ω} is the sum of all ohmic losses which are proportional to the generated current I , and the ohmic resistance of the system, R_{Ω} . [1]

$$E_{MFC} = E_{emf} - \left(\sum \eta_a + \left| \sum \eta_c \right| + IR_{\Omega} \right) \quad (4.8)$$

The overpotentials of the electrodes are generally current dependent, and in an MFC, they can roughly be categorised as activation losses, bacterial metabolic losses and mass transport or concentration losses. A symmetrical semi-cycle power density curve is typical for a high internal resistance MFC limited by ohmic resistance (dashed line in the right graphic of Figure 4.1) rather than a fuel cell defined by mass transfer (solid line in the same graphic of Figure 4.1). [1]

4.1.6. Coulombic efficiency

Continuing the parameters studied in MFCs, Coulombic efficiency is defined as the ratio of total Coulombs transferred to the anode from the substrate to maximum possible Coulombs if all substrate removal produced current. The total Coulombs obtained is determined by integrating the current over time so that the Coulombic efficiency for an MFC run in fed-batch mode, ε_{Cb} , evaluated over a time period, tb . And is calculated by Equation (4.9), where $M = 32$ because is the molecular weight of oxygen, F is Faraday's constant, $b = 4$ is the number of electrons exchanged per mole of oxygen, v_{An} is the volume of liquid in the anode compartment, and ΔCOD is the change in COD over time tb .

$$\varepsilon_{Cb} = \frac{M \int_0^{tb} I dt}{Fbv_{An}\Delta COD} \quad (4.9)$$

The utilisation of alternate electron acceptors diminishes the Coulombic efficiency by the bacteria, either those present in the medium, or those diffusing through the CEM such as oxygen. Other factors that reduce Coulombic efficiency are competitive processes and bacterial growth. Bacteria unable to utilise the electrode as an electron acceptor are likely to use substrate for fermentation or methanogenesis. [1]

4.1.7. Loading rates

Another parameter is useful to examine performance achieved with MFCs in terms of loading rates with those typically obtained in conventional treatment systems. To do this is calculated the loading based on m^3 d-volumetric loading rates. [1]

4.1.8. Energy recover

Finally, the most critical factor for evaluating the performance of an MFC for making electricity, compared to more traditional techniques, is to assess the system in terms of energy recovery. The overall energetic efficiency, ε_E , is calculated as the ratio of power produced by the cell over a time interval, t , to the heat of combustion of the organic substrate added in that time frame or as is on Equation (4.10) where ΔH is the heat of combustion in J/mol^{-1} and m_{added} is the amount in mol of substrate added.

$$\varepsilon_E = \frac{\int_0^t E_{MFC} I dt}{\Delta H m_{added}} \quad (4.10)$$

In MFCs, energy efficiencies range from 2% to 50% or more when easily biodegradable substrates are used. [1]

4.2. Study examples

Study MFCs with a potentiostat has been done with the evaluation of the parameters already explained through electrochemical techniques. For elucidation proposes some examples will be provided next.

The work described in [21] examines the impact of carbonate buffer (CB) concentration on anode performance using three methods to obtain a wide range of current densities, such as chronoamperometry, LSVs, and potentials in polarisation curves. CBs have been proposed as a more favorable alternative to phosphate buffers for microbial electrochemical experiments in laboratory studies, and it is more relevant to wastewater tests as the buffer capacity of a wastewater is dependent by its bicarbonate alkalinity and not the phosphate ion concentration. However, the impact of CBs, especially at higher concentrations, has not been well investigated relative to anode or MFC performance compared to phosphate buffers. A carbonate buffer can be better for anode performance, and it has higher pKa's than a phosphate buffer. Being pKa the number that shows how weak or strong an acid is.

Methods for MFC performance analysis, based on power density curves, are also a possibility in [21]. In this study were analysed by polarisation data obtained using LSVs with the electrode potential slope (EPS) method to quantify the individual anode and cathode resistances in the different buffer solutions at different concentrations of CB. The EPS method, in resume, quantifies component-associated resistances.

LSV was conducted on the anode electrode at a scan rate of 0.1 mV s⁻¹ from the open circuit potential (OCP) to +200 mV vs SHE while also measuring the correspondent cathode potential. Besides that, it was calculated the solution resistance between anode and reference electrode. At the end of the LSV, the solution resistance between the RE and the cathode was measured with other technique, EIS. The reported electrode potentials were corrected based on the solution resistance between each electrode and the RE.

The linearised portion of the electrode potential near the peak power density can be used to assess anodic and cathodic potentials under the experimental conditions to describe better the electrode performance in terms of practical electrode potentials rather than open-circuit potentials. The slopes of the linearised portion of the electrode potentials were used to calculate the anode and cathode resistances, with the solution resistance as the third component of the total internal resistance of the cell. Thus, the linearised portion of the electrode potentials, from the polarization curves, as a function of the current density, was fit to $E = mj + b$, Where j is the current density. The slope m is defined as the specific resistance of the anode or cathode in units of $m\Omega m^2$, and the y-intercepts are used to calculate the experimental open-circuit potentials of the anode or cathode. Some of the parameters studied were also maximum current densities in polarisation tests. The linearization of the data from polarization tests was used to calculate the MFC internal resistance and to calculate anode and cathode resistances. The parameters studied are presented in Figure 4.2.

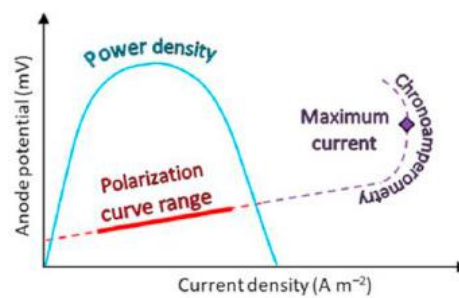


Figure 4.2: Parameters studied, from [21].

A series of equations explicitly shows how electrode potentials can be corrected to ensure more accurate reporting of electrode potentials, such as how maximum power densities are impacted by solution ohmic resistance was developed in [22]. The resistances needed to make these adjustments can be obtained by simply measuring the distances between electrodes using the solution conductivity or using a more advanced approach such as EIS.

A fact is that cylindrical brush anodes generally produced higher current densities than flat carbon felt, carbon cloth, and carbon paper anodes when coupled to a cathode with a platinum catalyst. Placing the electrodes close to each other should improve power production as it reduces ohmic resistance. Accurate measurement of electrode potentials is important for knowing how changes in electrode materials or electrode spacing alter performance.

Many studies have shown in acetate fed MFCs that the cathode potential decreases more rapidly with current than the brush anode potential, which indicated that the cathode was limiting power production. However, conclusions concerning which electrode defines power production require accurate measurements of the electrode potentials, particularly at higher current densities in solutions with low conductivities.

The distances between REs and WEs are usually not reported, confounding an analysis to calculate true electrode potentials. From an electrochemical perspective, the RE should be placed as close as possible to the WE, but it is not clear what portion of the brush surface should be used when using a brush anode. In an MFC with a single RE, the cathode potential is often calculated as the difference between the anode potential and the whole-cell potential.

In other studies, only one RE is used to report electrode potentials. If there is an appreciable distance between the WE and the RE, then the measured electrode potentials will include ohmic drop due to ohmic resistance, which is a current function. Assuming that the WE is the anode, its potential is corrected for the ohmic resistance using a single RE and can be estimated using the measured potential as in Equation (4.11), where d_{An-RE} is the distance in cm between the anode and the RE, and i is the current in A,

$$E_{AnRE} = E_{An} - \left(\frac{10^3 R_{\Omega} d_{An-RE}}{l} \right) i. \quad (4.11)$$

A traditional potentiostat will automatically correct the anode potential for ohmic resistance, which would be $E_{AnRE} = E_{An}$. For calculating the cathode potential, one approach, when using one RE, is to use the cathode as the working electrode when obtaining polarisation data. In this case, the cathode potential would also be calculated using Equation (4.11) with the distance defined as d_{Cat-RE} .

The correct distances to use for the equations can be difficult to estimate for large and highly porous electrodes such as graphite fibre brush electrodes or thick carbon felt, as it is not clear whether the distance should be from the edge of the electrode or the middle of the electrode. In this work, it was used the distance between the closest edges of the anode and cathode. A schematic description of an MFC is presented in Figure 4.3, and is a brush anode MFC with the RE placed inside the electric field and at a distance smaller than 0.2 cm to the WE.

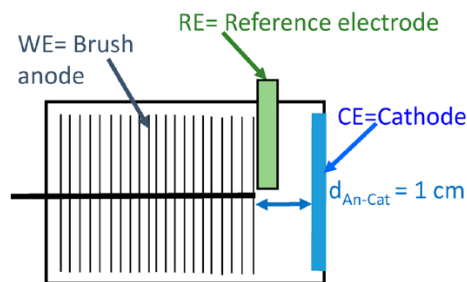


Figure 4.3: Schematic of a MFC type (from [22]).

In the majority of MFC studies, the distances between the RE and WE or even the method to calculate the cathode potentials have not been reported, but as shown in this work, the solution conductivity can be used to estimate the ohmic resistance just based on measured spacing between the RE and a working electrode or the distance between the anode and cathode, as the ohmic resistances obtained from measured distances agreed well with measurements made using EIS. [22]

Another work where the MFC is studied is presented in [23]. Several different configurations were used to examine the effect of different electrode positions and reactor geometry on electrochemical characterisation of the bio anodes. More specifically, anodes were placed horizontally in the MFC cylindrical chamber with the brush core 0.5 cm from one cube edge.

In the Spaced electrode assembly -3 (SPA) MFCs, one of the configurations, reactors were constructed using three 2 cm-cube segments with the two electrodes placed at the two ends. The cathode was 5.5 cm away from the anode brush core. The Separator Electrode Assembly -3 (SEA) similarly had three segments, but the cathode was placed 0.5 cm away from the anode brush core, with two layers of a porous cloth separator used to prevent electrode short-circuiting. The RE was inserted through the middle hole of the 2 cm-cube segments, so that the RE had three candidate positions of 1 (nearest to the anode, 0.5 cm horizontal distance from the brush core), 2 (in the middle segment, 2.5 cm from the brush core), and 3 (farthest, 4.5 cm from the brush core) during the experiments.

The physical spacing between the RE and the anode for each position was kept the same for the SPA-3 and SEA-3 MFC. To examine the effect of reactor configuration on the measurements, a schematic of these two configurations is in Figure 4.4.

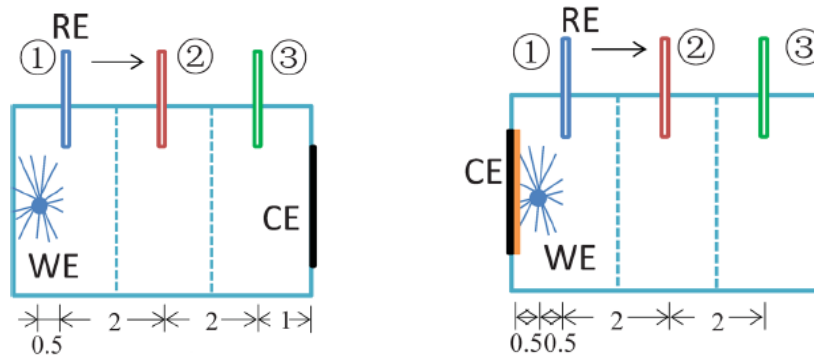


Figure 4.4: MFCs schematic, SPA (left) and SEA (right) (from [23]).

Electrochemical tests were all performed with anodes as the WE and cathodes as the CE using a potentiostat. EIS tests were conducted at anode polarised potentials of -0.2 and -0.15 V vs SHE, over a frequency range of 100 kHz to 5 mHz with a sinusoidal perturbation of 10 mV amplitude.

The spectra were fitted into an equivalent circuit, presented in Figure 4.5, using a software application to obtain the uncompensated ohmic resistance (R_u), charge transfer resistance (R_{ct}), and diffusion resistance (R_d).

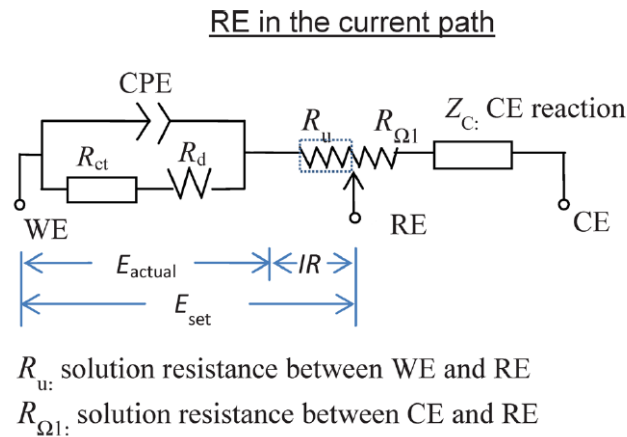


Figure 4.5: Simplified schematic circuit for 3-electrode setup (from [23]).

4.3. Dummy cells

A dummy cell is a network of known resistors, capacitors or inductors used to test or calibrate a potentiostat to ensure that is working correctly. The dummy cell is used in place of an existing electrochemical system when troubleshooting a potentiostat. The dummy cell provides a known response, whereas various chemical phenomena may complicate the response from a physical electrochemical system. [24]

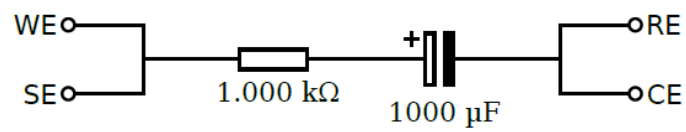


Figure 4.6: Schematic diagram of a dummy cell (from [24]).

Chapter 5

5. Potentiostat development

The following chapter will explain the schematic of a low-cost potentiostat made in a PCB, with each component description. Further, it presents the man-machine interface developed and the implemented firmware.

5.1. Circuit development and electronics assembly

5.1.1. DAC

A digital-to-analogue converter (DAC) outputs an electrical signal representing the desired potential, in the potentiostatic mode, or the desired current, in the galvanostatic mode. An operational amplifier compares this to the measured potential or the measured current and drives current into the CE until the measured value equals the DAC setpoint. Both the measured potential and the measured current are fed into an analogue-to-digital converter (ADC) for data acquisition purposes. [25]

The model chosen to use in the potentiostat was DAC8531, which is a low-power, single, 16-bit buffered voltage output DAC. Its on-chip precision output amplifier allows rail-to-rail output swing to be achieved. It uses a versatile three-wire serial interface that operates at clock rates up to 30MHz and is compatible with standard Serial Peripheral Interface (SPI), Quad Serial Peripheral Interface, Microwire, and Digital Signal Processor interfaces. The schematic of this is in Figure 5.1.

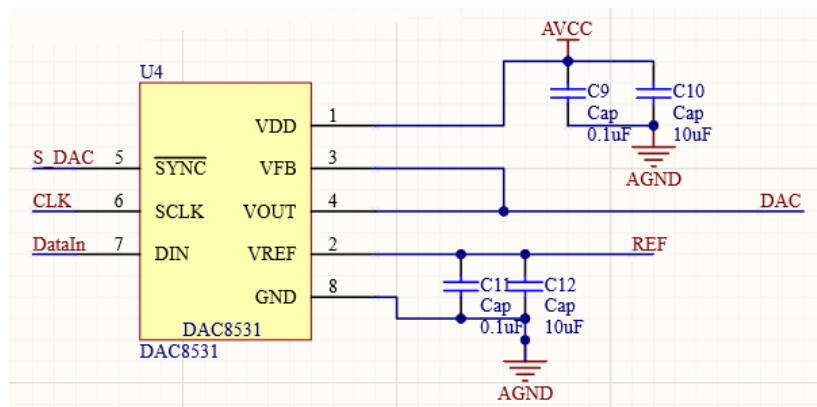


Figure 5.1: DAC8531 schematic.

Also, in Figure 5.1, it is possible to see in evidence the pin configuration of this model, described in Table 5.1.

Table 5.1: Pin description for DAC8531 (adapted from [25]).

| Pin | Name | Function |
|-----|-------------------|---------------------------------------------------------------------------------------|
| 1 | VDD | Power supply input (ranges from 2.7 to 5.5 V). |
| 2 | VREF | Reference voltage input. |
| 3 | VFB | Feedback connection for the output amplifier. |
| 4 | VOUT | The analog output voltage from DAC. |
| 5 | \overline{SYNC} | Level-triggered control input is the frame synchronization signal for the input data. |
| 6 | SCLK | The serial clock input (at rates up to 30 MHz). |
| 7 | DIN | Serial data input clocked into a 24-bit shift register the falling edge of the SCLK. |
| 8 | GND | A ground reference point for all circuitry. |

The DAC8531 requires an external reference voltage to set the output range of the DAC. Also, it incorporates a power-on reset circuit that ensures that the DAC output powers up at 0 V and remain there until a valid write takes place to the device. It contains a power-down feature, accessed over the serial interface, that reduces the device's current consumption to 200 nA at 5 V. The low power consumption of this part, in normal operation, makes it ideally suited to portable battery-operated equipment. The power consumption is 2 mW at 5 V reducing to 1 μ W in power-down mode. [25]

5.1.2. ADC

The ADCs, in a simple way, translate analogue quantities to digital language, used in information processing, computing, data transmission, and control systems.

The ADS8331 was the ADC chosen to integrate the potentiostat. The device has low-power operation, 16-bit, 500-k samples-per-second ADC with a unipolar, 4-to-1 multiplexer (MUX) input. The device includes a 16-bit capacitor-based successive approximation register ADC with inherent sample and hold. Figure 5.2 shows the respective schematic. [26]

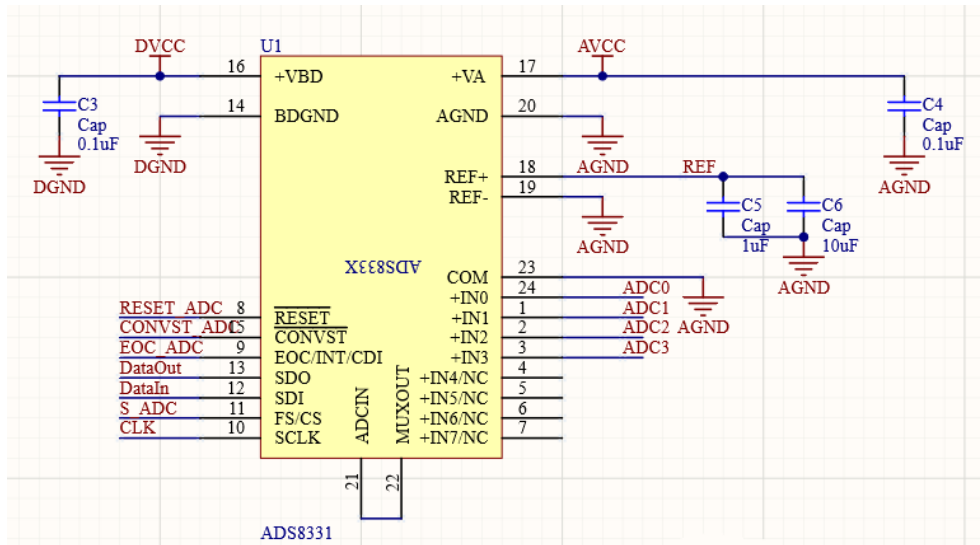


Figure 5.2: ADS8331 schematic.

In evidence is the pin configuration, more detailed in Table 5.2.

Table 5.2: Pin description of ADS8331 (adapted from [26]).

| Pin | Name | Function |
|--------|-------------|-----------------------------------------------------------------------------------------|
| 1-3,24 | IN[0-3] | Mux inputs. |
| 4-7 | NC | No connection. |
| 8 | RESET | External reset. |
| 9 | EOC/INT/CDI | Status output. The polarity of EOC or INT is programmable. Chain data input if used. |
| 10 | SCLK | SPI clock for the serial interface. |
| 11 | FS/CS | Frame sync signal for DSP or chip select input for SPI. |
| 12 | SDI | SPI serial data in. |
| 13 | SDO | SPI serial data out. |
| 14 | DGND | Digital interface ground. |
| 15 | CONVST | Conversion start. |
| 16 | +VBD | Digital interface supply. |
| 17 | +VA | Analogue supply (2.7 to 5.5 V). |
| 18 | REF+ | External reference input. |
| 19 | REF- | External reference ground connected to AGND. |
| 20 | AGND | Analogue ground. |
| 21 | ADCIN | ADC input. |
| 22 | MUXOUT | Mux output. |
| 23 | COM | Standard ADC input, connected to AGND. |

5.1.3. Optical isolators

Two optical isolators were added to prevent noise. An opto-isolator is an electronic component that transfers electrical signals between two isolated circuits using light. It is designed to allow the optical signal to travel in the forward direction while block reflections that travel in the backward direction.

The components chosen were ISO7240 and ISO7242. This family is quad-channel digital isolators with multiple channel configurations, and output enables functions. These devices have logic input and output buffers separated by a silicon dioxide isolation barrier. In conjunction with isolated power supplies, these devices block high voltage, isolate grounds, and prevent noise currents from entering the local ground, interfering with or damaging sensitive circuitry. The ISO7240 has all four channels in the same direction, by the other side, ISO7242 has two channels in each direction. [27] The schematic of both components is in Figure 5.3.

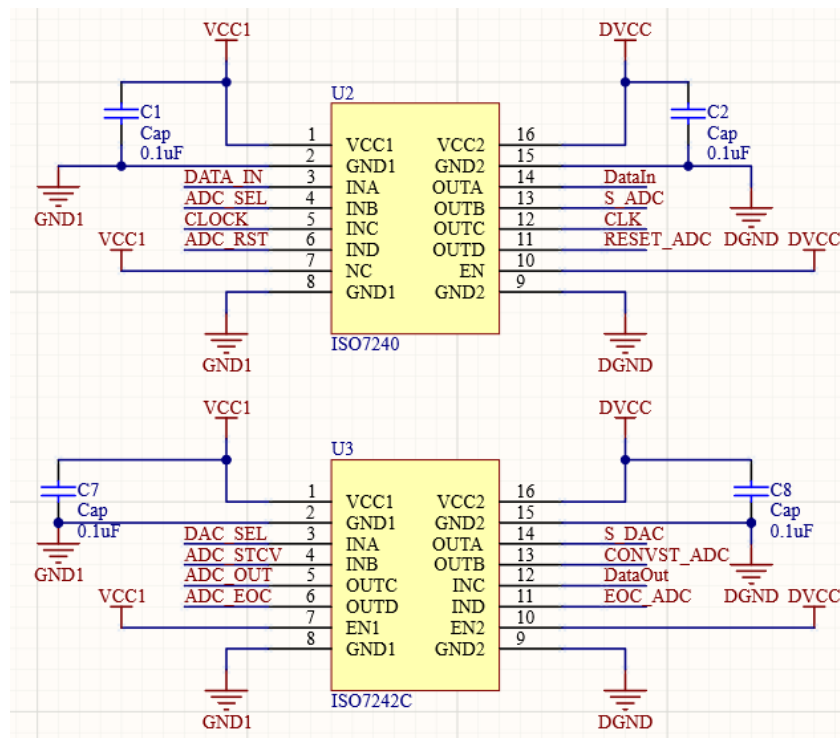


Figure 5.3: Schematic of ISO7240 and ISO7242.

Each pin configuration is detailed in Table 5.3.

Table 5.3: Pin configuration for ISO family (adapted from [27]).

| Pin | | Name | Function |
|---------|---------|----------|-------------------------------------------------------------|
| ISO7240 | ISO7242 | | |
| 1 | 1 | VCC1 | Power supply. |
| 2,8 | 2,8 | GND1 | Ground connection for VCC1. |
| 3-6 | 3-6 | IN[A-D] | Input, for respective channel number [A-D]. |
| 7 | - | NC | No connected pins are floating with no internal connection. |
| - | 7 | EN1 | Output enabled 1. |
| 9,15 | 9,15 | GND2 | Ground connection for VCC2. |
| 10 | - | EN | Output enabled for all pins. |
| - | 10 | EN2 | Output enable 2, for pins on side-2. |
| 11-14 | 11-14 | OUT[A-D] | Output, for respective channel number [A-D] |
| 16 | 16 | VCC2 | Power supply. |

5.1.4. Potentiostat system

The general schematic representation of the potentiostat system used is represented in Figure 5.4.

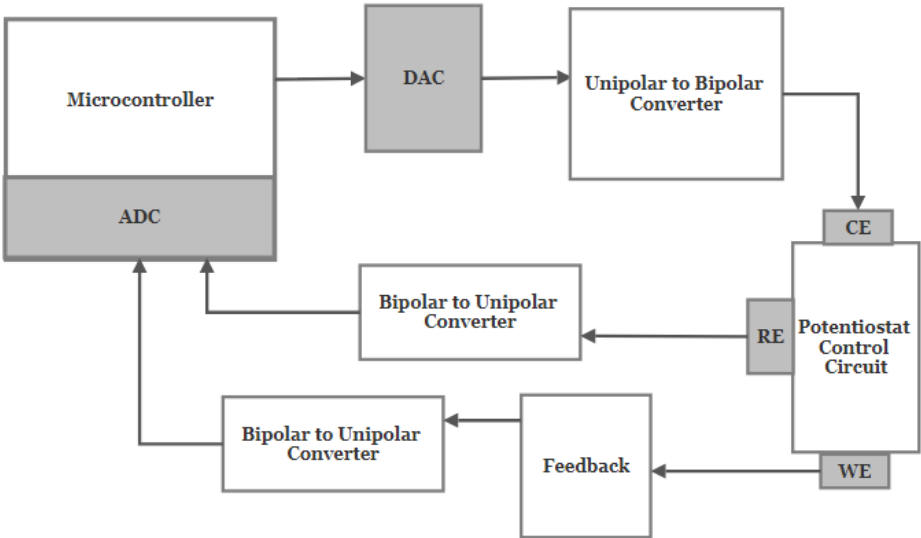


Figure 5.4: Potentiostat system.

The ADC acquires data from the analogue domain and converts it to the digital domain making it available to be process by the firmware. Level shifters make a theoretical bridge between different segments of the circuit. These were configured as bipolar-to unipolar converters and unipolar-to-bipolar converters. The level shifters transform a voltage signal produced in one circuit module into a form required in another. [28]

A javascript software interface was developed in node-red for data acquisition and control of the circuit. The data acquired were exported to the spreadsheet program for detailed analysis.

The potentiostat control circuit is presented in Figure 5.5 in more detail and divided in four parts, described as it follows.

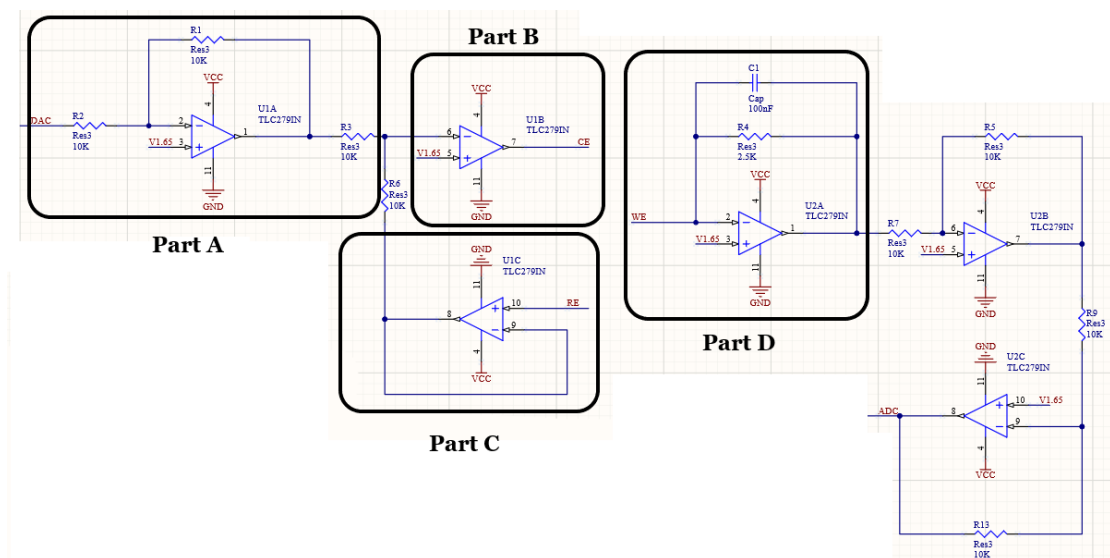


Figure 5.5: Potentiostat control circuit.

Part A

This is a differential amplifier. The Op-amp amplifies the voltage difference between the non-inverting input and the inverting input. If all the resistors have the same value, then the circuit becomes a unity gain differential amplifier.

Part B

In this part, the voltage output from part A is fed into the non-inverting input of Op-amp 2 while the Op-amp's inverting input was directly connected to its output. Op-amp 2 was

configured as a voltage follower. This isolates the input from the output to prevent loading of the input signal. The voltage output from Op-amp 2 was connected to the CE.

Part C

This contains Op-amp 3 configured as a voltage follower. This is an additional measure to prevent current flow through the RE.

Part D

This last part is the current measurement part based on the feedback ammeter principle.

Electrochemical cell is in evidence in Figure 5.6.

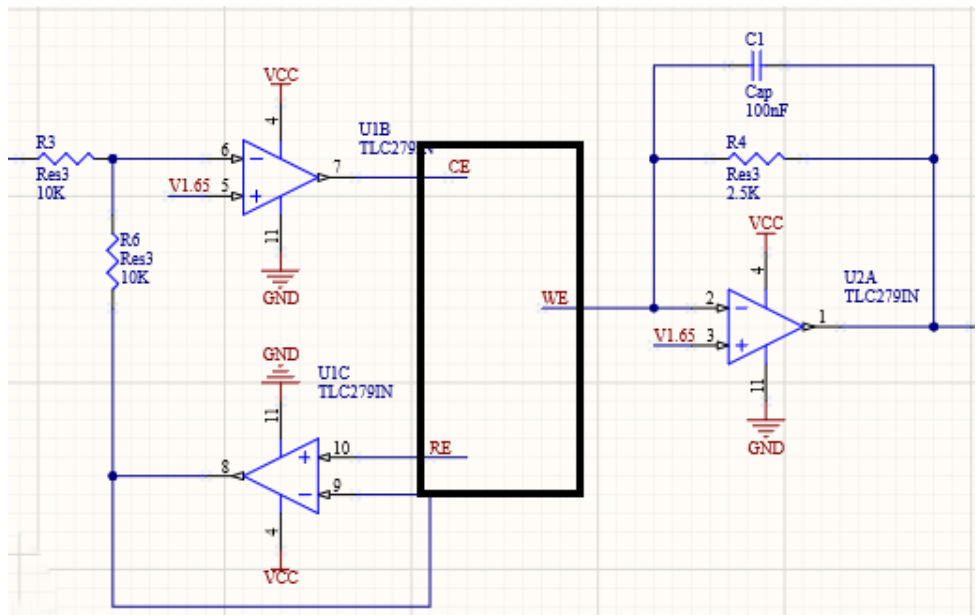


Figure 5.6: Electrochemical cell.

5.2. Functional overview of the system

Based on the theoretical background presented above, we have developed an interface for monitoring a MFC reactor using Node-RED. Figure 5.7 shows the architecture of our system.

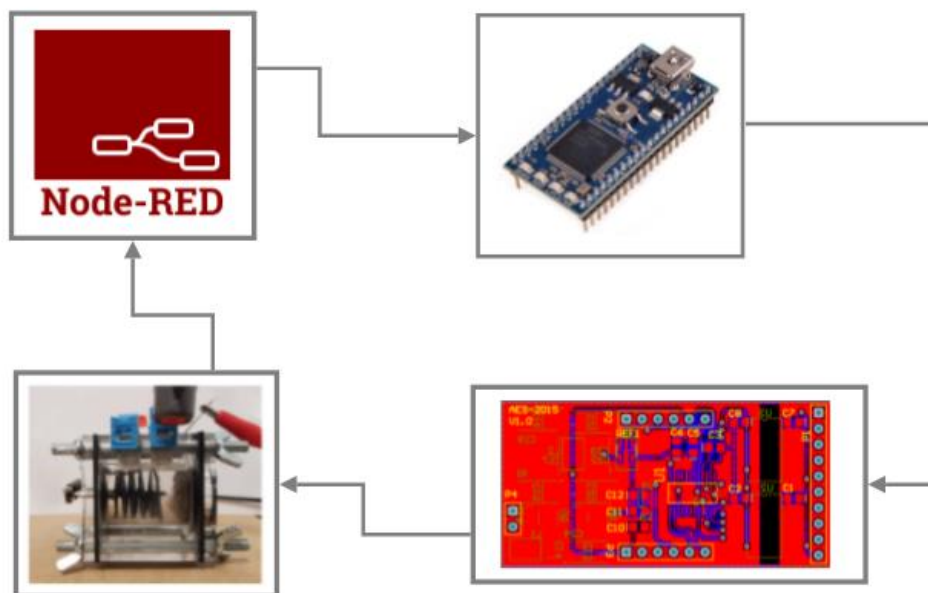


Figure 5.7: Overview of the setup (adapted from [29], [30], [31]).

5.3. Man-machine interface with Node-RED

The software interface used was Node-RED, an open-source JavaScript-based development environment based on Node.js, developed by IBM engineers and most suitable for developing IoT systems. It is a process-based virtual programming environment that creates data streams from the sensor to the computer by connecting hardware and software. It can compile data processing logic easily and transfer the process data to higher-level systems in minutes or display it immediately. Instead of programming a web page displaying different sensor data, Node-RED provides a Dashboard interface that allows the creation of an interface without advanced knowledge in programming languages. [30]

To understand the interface, it will be broken down in each step and function used, explaining the purpose and showing the blocks. First of all, the aim is to inject input parameters, save them in a global variable to use later and finally display in a chart and store them in a text file, as it is described in the scheme of Figure 5.8.

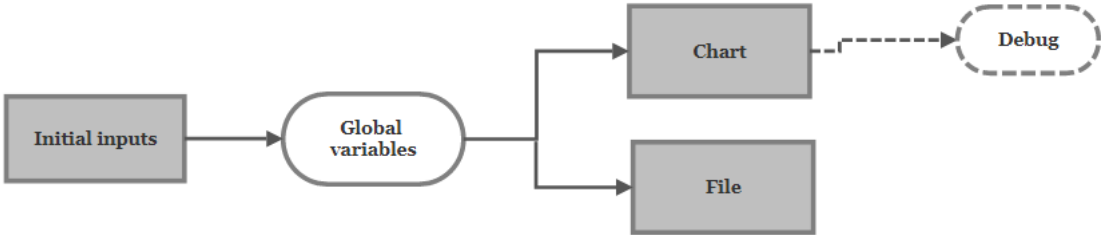


Figure 5.8: Input parameters block in a scheme.

The initial inputs and values tested are listed in Table 5.4.

Table 5.4: Input parameters.

| Input parameter | Example values |
|------------------------------|----------------|
| Duration of experience (sec) | 60 |
| Cycle period (sec) | 30 |
| Number of points | 100 |
| VCE maximum (mV) | 2 |
| VCE minimum (mV) | 1 |

The duration of the experience is the time established to the total time of the experience. Cycle period, is characterize by the complete repetition of the pattern in a periodic function, in terms of y-values at regular intervals, so in short, the period of a function is

Finally the result is presented as it follows in Figure 5.11, the dashboard version and the file result.

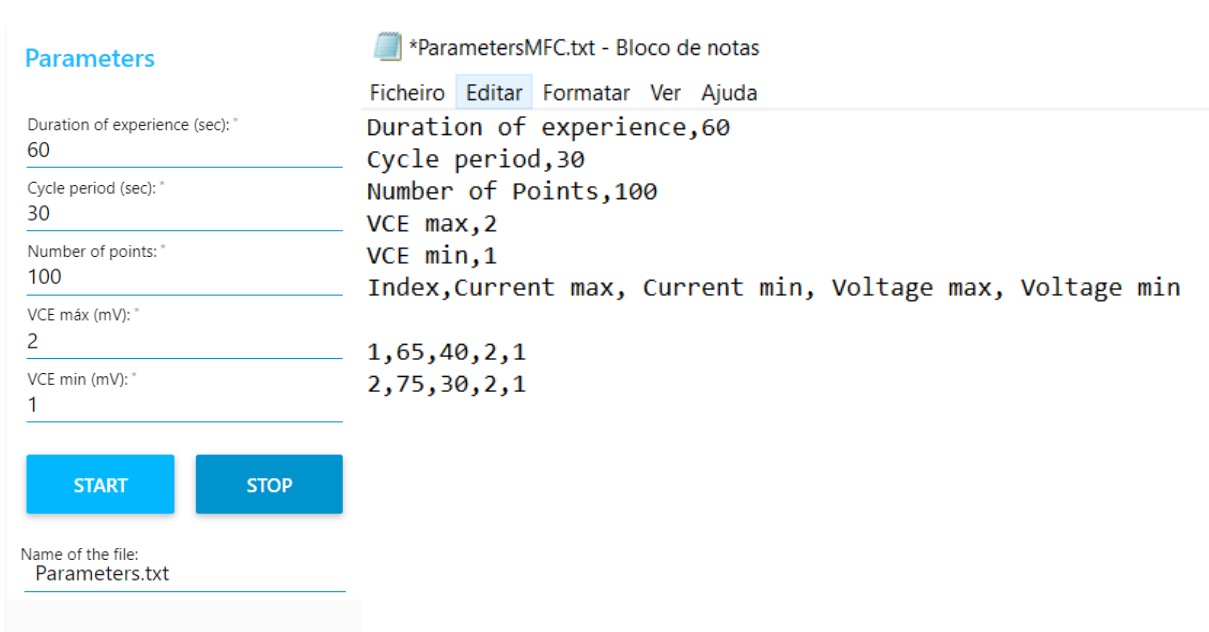


Figure 5.11: File result.

The second part of the flow is described in a explicative scheme, in Figure 5.12.

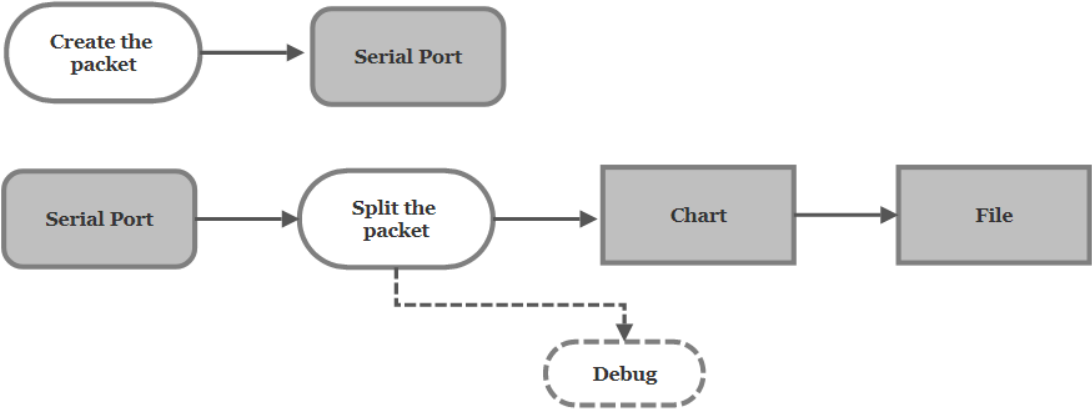


Figure 5.12: Scheme relative to Serial Port interaction in Node-RED.

In order to visualize the global flow, is in Figure 5.13 other part created, concerning to the packet of data created and its transmission to the mbed DAC. Then, is carried out the reception of other packet from the mbed ADC that will update the existed data in parameters file, and finally is displayed the information in a chart. Finally, is saved the data from the chart in other file to posterior analysis and discussion.

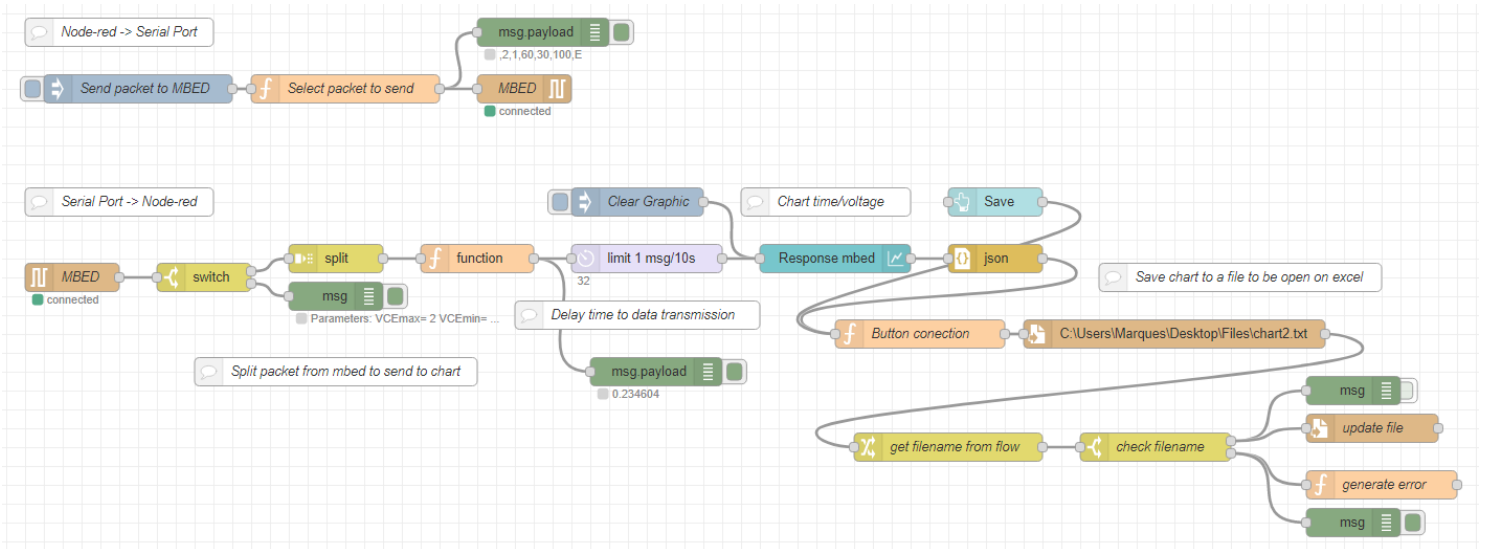


Figure 5.13: Second part of the flow, interaction with serial port.

Two functions used to clarify the flow above, presented in Figure 5.14. The first one is relative to the selection of the packet to send, where are used the input values previously saved and structured by a division of commas and an end character to define the packet end, in this case, is the letter “E”. The second part is the function code to make the button connection of the “Save” button to store the data by clicking the button directly in the dashboard.

```

1 var parameters = global.get("Values");
2
3 var final= ','+parameters.VCEmax+', '+parameters.VCEmin+', '+parameters.Duration+', '+parameters.Cycle+', '+parameters.Points+', '+ 'E';
4
5 msg.payload= final;
6
7 return msg;

```

Name: Button conection

Function

```

1 if (msg.topic === "save") {
2   msg.payload = context.last;
3   return msg;
4 }
5 else {
6   context.last = msg.payload;
7 }
8 return null;

```

Figure 5.14: Functions of the second part of the flow.

Finally, to obtain an x/y axis chart, some exchanges had to be done, shown in Figure 5.15, because the default charts have an x-axis in the time base.

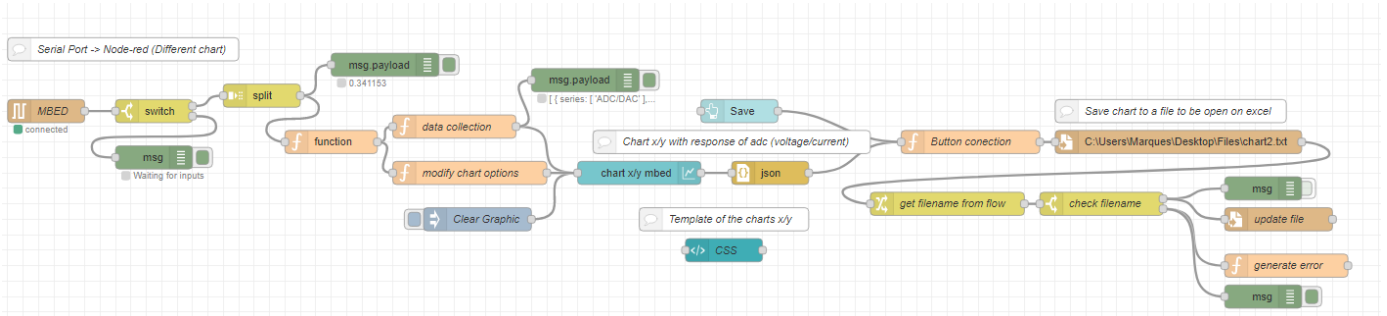


Figure 5.15: Flow for the chart with x/y axis.

The difference between the previous flow is the configurations to the chart node and creating a template for all the charts to make it more appealing. It is in evidence the function blocks in Figure 5.16

| Name | Function |
|---------------------------------------------------------------------------------------------------------------------------------------------------------------------------------------------------------------------------------------------------------------------------------------------------------------------------|--------------------------------------------------------------------------------------------------------------------------------------------------------------------------------------------------------------------------------------------------------------------------------------------------------------------------------------------------------------|
| <p>Setup</p> <pre>1 global.set("Data_mbed", msg.payload); 2 return msg;</pre> <p>Template type: Added to site <head> section</p> <p>Name: CSS</p> <p>Template</p> <pre>1 <style> 2 canvas.chart.chart-line { 3 height:calc(100%) !important; 4 width: calc(100%) !important; 5 } 6 7 </style></pre> | <p>Setup</p> <pre>1 var Data = global.get("Data_mbed"); 2 3 //var index = msg.parts.index+1; 4 5 data = [{x:0,y:Data}, 6 {x:1,y:Data}, 7 {x:2,y:Data}]; 8 9 msg.payload= [{ 10 "series": ["ADC/DAC"], 11 "xAxisID": 'custom-x-axis', 12 "yAxisID": 'custom-y-axis', 13 "data": [data], 14 "labels": [""] 15 ^}] 16 17 return msg;</pre> |

```

1 let gridcolors = 'rgba(255, 160, 0, 0.3)'
2 msg.ui_control = {
3   options: {
4     legend: {
5       display: true
6     },
7     tooltips: {
8       enabled: true
9     },
10    scales: {
11      xAxes: [{
12        type: 'linear',
13        id: 'custom-x-axis',
14        position: 'bottom',
15        padding:100,
16        gridLines:{
17          color:gridcolors,
18          zeroLineColor:'rgba(123, 113, 113, 0.75)',
19          tickMarkLength:7,
20          drawTicks:true
21        },
22        ticks: {
23          fontColor:"#111",
24          max: 5,
25          min: 0,
26          stepSize: 1
27        }
28      }
29    }
30  }

```

Figure 5.16: Block functions to explain the steps added.

First is the data selection in the packet, then the data is modified to define the x axis, change the colours, and a general template for all the charts in the interface.

To visualize all the interface is in Figure 5.17 the dashboard and in Figure 5.18 the whole flow.

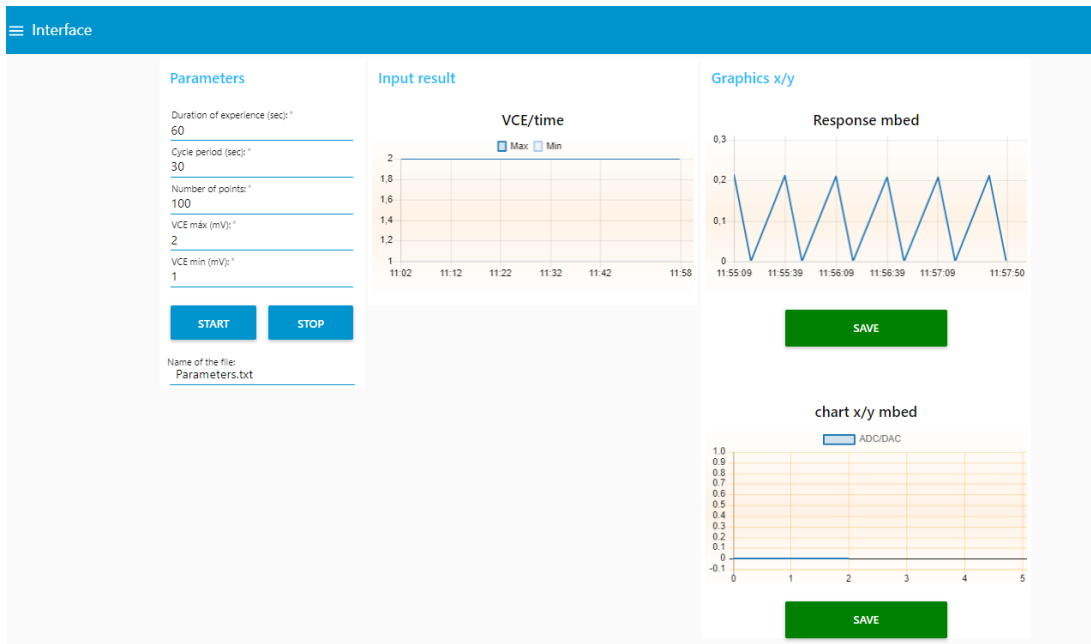


Figure 5.17: Dashboard of Interface.

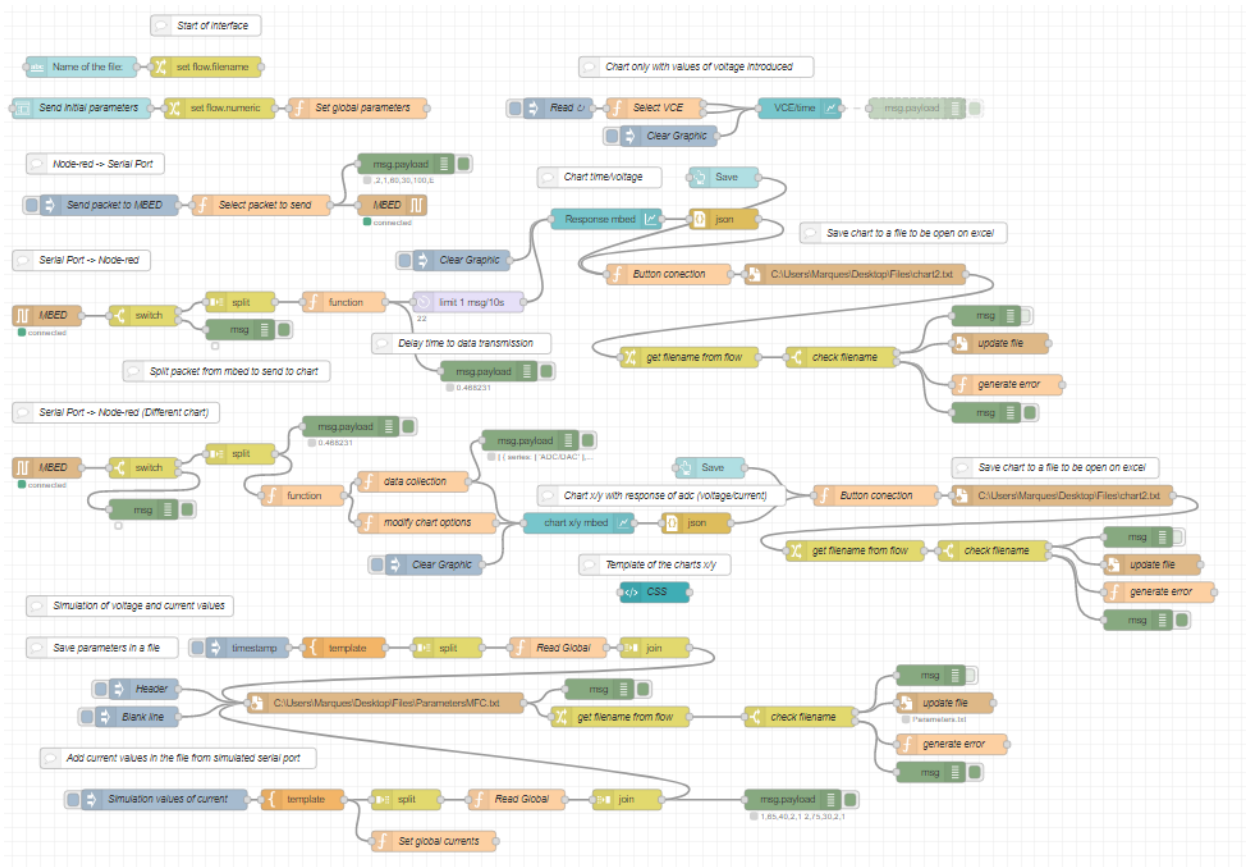


Figure 5.18: Full flow.

5.4. Firmware development

A mbed microcontroller connects the Node-RED with the potentiostat to transmit and receive the information making use of this device the code in mbed was tested.

The mbed Compiler provides a lightweight online C/C++ IDE that is pre-configured to write programs quickly, compile and download them to run on the mbed Microcontroller. Do not demand installing or set up anything to get running with mbed. Because it is a web app, it is possible to login from anywhere and continues to work. [31]

5.4.1. MBED LPC1768

The mbed Microcontrollers are a series of ARM microcontroller development boards designed for rapid prototyping. The mbed microcontroller chosen to use was NXP LPC1768, that is in particular designed for prototyping all sorts of devices, especially those including Ethernet, USB, and the flexibility of lots of peripheral interfaces and FLASH memory. It is packaged as a small DIP form-factor for prototyping with through-hole PCBs, stripboard and breadboard, and includes a built-in USB FLASH programmer. The pinout diagram for this mbed is presented in Figure 5.19.

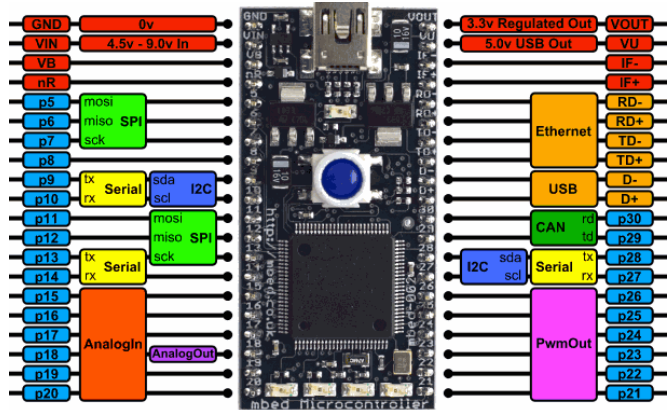


Figure 5.19: Pinout diagram of mbed NXP LPC1768 board (from [31]).

The pins used for testing the intern ADC and DAC were pin 15 and pin 18, respectively.

5.4.2. SPI communication

The SPI provides an SPI Master that connects to an SPI Slave and manages the communications. This interface protocol establishes the communication with SPI Slave devices, such as FLASH memory, LCD screens, and other modules or integrated circuits.

The mbed has two SPI ports, each one supporting Master or Slave operation. The API summary for SPI Master is shown in Table 5.5. The same pin is used for SDI if in Master mode, or SDO if Slave on many other devices. Hence this pin gets to be called MISO (Master In, Slave Out). Its partner pin is MOSI (Master Out, Slave In). [32]

Table 5.5: API summary for SPI Master (adapted from [32]).

| Functions | Description |
|-----------|-------------------------------------------------------|
| SPI | Create an SPI master connected to the specified pins. |
| format | Configure the data transmission mode and data length. |
| frequency | Set the SPI bus clock frequency. |
| write | Write to the SPI Slave and return the response. |

The mode is another feature of SPI which allows the choice of which clock edge is used to clock data into the shift register and whether the clock idles high or low.

5.4.3. MBED software

The goals with the mbed firmware were to validate communication between Node-RED and mbed, as shown in the diagram of Figure 5.20. In this situation, microcontroller's internal ADC and DAC operation were evaluated and visualised with the oscilloscope.

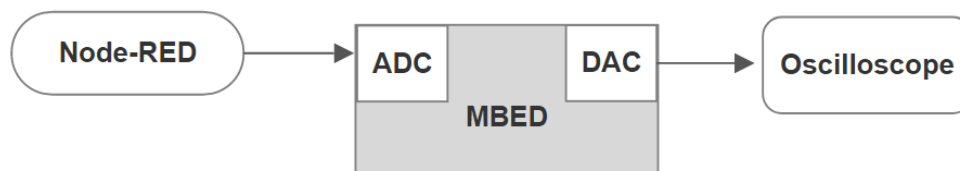


Figura 5.20: Diagram of mbed communications.

For validation purposes, parts of the mbed firmware will be presented with the main parts in evidence. Firstly a routine that scrolls through the list of data coming from Node-RED, the data package structure is explained before. Starting from the end character “E”, the counter decrements until the first value of the list. In the end, the packet is returned

to the Node-RED debug console using the printf command to confirm that the data was correctly received in mbed. All these instructions are set in Figure 5.21.

```

45 //*****
46 // PC serial port receive event function
47 //*****
48 void pc_serial_RX_interrupt(void)
49 {
50     led2 = 1;
51     if(buffer_PC_RX[buffer_PC_RX_ptr] < PC_BUFFER_RX_SIZE) {
52         buffer_PC_RX[buffer_PC_RX_ptr] = pc.getc();
53
54         if (buffer_PC_RX[buffer_PC_RX_ptr] != 'E'){
55             buffer_PC_RX_ptr++;
56         }
57         else{
58             buffer_PC_RX_ptr--;
59             buffer_PC_RX_ptr--;
60
61             char p = 1;
62             P = 0;
63             while (buffer_PC_RX[buffer_PC_RX_ptr] != ','){
64                 P = P + (buffer_PC_RX[buffer_PC_RX_ptr] - 0x30)*p;
65                 p = p*10;
66                 buffer_PC_RX_ptr--;
67             }
68
69             p = 1;
70             buffer_PC_RX_ptr--;
71             Tc = 0;
72             while (buffer_PC_RX[buffer_PC_RX_ptr] != ','){
73                 Tc = Tc + (buffer_PC_RX[buffer_PC_RX_ptr] - 0x30)*p;
74                 p = p*10;
75                 buffer_PC_RX_ptr--;
76             }
77
78             p = 1;
79             buffer_PC_RX_ptr--;
80             Tp = 0;
81             while (buffer_PC_RX[buffer_PC_RX_ptr] != ','){
82                 Tp = Tp + (buffer_PC_RX[buffer_PC_RX_ptr] - 0x30)*p;
83                 p = p*10;
84                 buffer_PC_RX_ptr--;
85             }
86
87             p = 1;
88             buffer_PC_RX_ptr--;
89
90             VCEmin = 0;
91             while (buffer_PC_RX[buffer_PC_RX_ptr] != ','){
92                 VCEmin = VCEmin + (buffer_PC_RX[buffer_PC_RX_ptr] - 0x30)*p;
93                 p = p*10;
94                 buffer_PC_RX_ptr--;
95             }
96
97             p = 1;
98             buffer_PC_RX_ptr--;
99
100             VCEmax = 0;
101             while (buffer_PC_RX[buffer_PC_RX_ptr] != ','){
102                 VCEmax = VCEmax + (buffer_PC_RX[buffer_PC_RX_ptr] - 0x30)*p;
103                 p = p*10;
104                 buffer_PC_RX_ptr--;
105             }
106             pc.printf("Parameters:\n VCEmax= %d\n VCEmin= %d\n Tp= %d\n Tc= %d\n P= %d\n", VCEmax, VCEmin, Tp, Tc, P);
107

```

Figure 5.21: Serial Port receive event function.

Next, the routine for data acquisition is presented in Figure 5.22. At this stage is wanted to verify if the signal reaches the oscilloscope, so we set commands to write in it.

```

108     DAC.write(0.5);           //*****
109                               // Routine of data acquisition
110     delta_V = VCEmax - VCEmin; //*****
111     float n = Tc/2/DAC_TICK;   void acquisition()
112     delta_V = (delta_V / n) / 3.3; {
113     direction = UP;           led1 = 1;
114
115     DAC.write(0);           if (direction == UP){
116                               DAC.write(DAC.read() + delta_V);
117     buffer_PC_RX_ptr = 0;
118     buffer_PC_RX_flag = SET;   if (DAC.read() >= VCEmax/3.3)
119     }                           direction = DOWN;
120     }                           }
121     else{                       else{
122     buffer_PC_RX_ptr = 0;       DAC.write(DAC.read() - delta_V);
123     }                           if (DAC.read() <= VCEmin/3.3)
124     led2=0;                     direction = UP;
125     }                           }
                                   led1 = 0;

```

Figure 5.22: Data acquisition routine.

This routine must be executed at a certain number of milliseconds, named the ticks of the system. In this case, was chosen one millisecond for the variable `DAC_TICK`. Also, the `delta_V` variable is initialised on the left side of Figure 5.22.

The ΔV , equivalent to the defined variable `delta_V`, increment must be calculated to obtain VCE maximum, after $T/2$ increments and starting in VCE minimum. It is $T/2$ because the number of interrupts of 1 millisecond since $T = 0$ until $T/2$ is equivalent to the middle of the chart. With this information, we obtain Equation (5.1),

$$\Delta V = \frac{VCE_{max} - VCE_{min}}{\frac{T}{2}} = 2 * \frac{(VCE_{max} - VCE_{min})}{T}. \quad (5.1)$$

Since the DAC has 10 bits of resolution, the possible options are $2^{10} = 1024$. And the system of mbed only supports until 3.3V, and the possible increment is $3300/1024 = 3.22$ mV.

The ADC obtains each sample with a a periode of T/N , being T the cycle period and N the number of points. If the $T = 60$ seconds and $N = 1000$ points, the value is 600 milliseconds.

The following step in developing mbed software was to validate the communication of mbed to an extern ADC and extern DAC, with the information coming from Node-RED, as it was in the first situation. A scheme explains it better, in Figure 5.23.

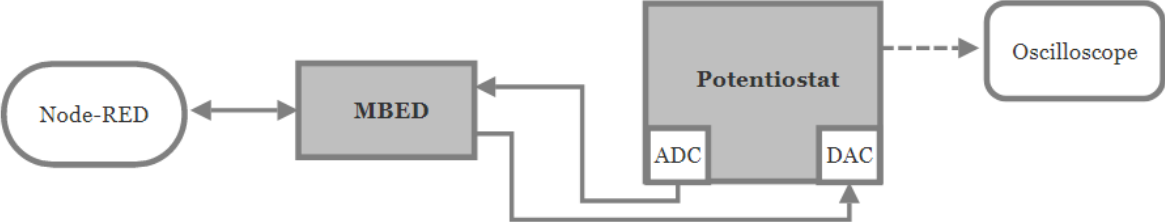


Figure 5.23: Comunnication with extern components.

For this purpose, it was written a code for SPI communication from mbed to an extern DAC. The next step, was to receive a response from the extern ADC, of the potentiostat.

Chapter 6

6. Methodology

This chapter consists of the intended protocol to follow before, during, and after experimental tests that would validate the hardware to study the MFCs with the potentiostat. Starting with the guidelines established then is described the tests chosen through simulation or experimentally, and finally some conclusions and information that would be expected to extract and discussed from the data collected.

6.1. Protocol guidelines

In order to study MFCs is necessary to take some steps that consist of a theoretic protocol to follow during the experiments. It can be divided like is described above.

Step 1

Prepare the working electrodes and counter electrodes that would be used—soaking membranes if needed. Then calibrate electrodes and make final verifications to prepare the MFC reactors fully.

Step 2

Set up the interface on the laptop used, test the hardware, make necessary calibrations, connect potentiostat. Perform a hardware check. Label the different MFCs, if they exist, type of samples and type of tests. Set up the electrochemical test chosen to do, for example, a cyclic voltammetry test.

Step 3

Make the tests on different days for different results. Save the data in files and represent it in the respective charts.

Step 4

Analyse the data in the interface through the graphics.

6.2. Simulation methodology

The simulation phase is essential to validate the hardware used, the potentiostat in this case, and obtain some results and conclusions in the impossibility of making experimental tests. To achieve a simulation should be made several measurements, described in the following subchapters.

6.2.1. Current measurement

A fixed potential or a fixed current may be set. This makes it possible to use the potentiostat as a constant-voltage or constant-current source. The resulting current, response voltage, will be continuously measured and displayed. [24]

Figure 6.1 shows an example of periodically changing the potential over the dummy cell between 0 V and +5V, green curve, resulting in some spikes that decay exponentially as expected for a resistor-capacitor circuit, red curve.

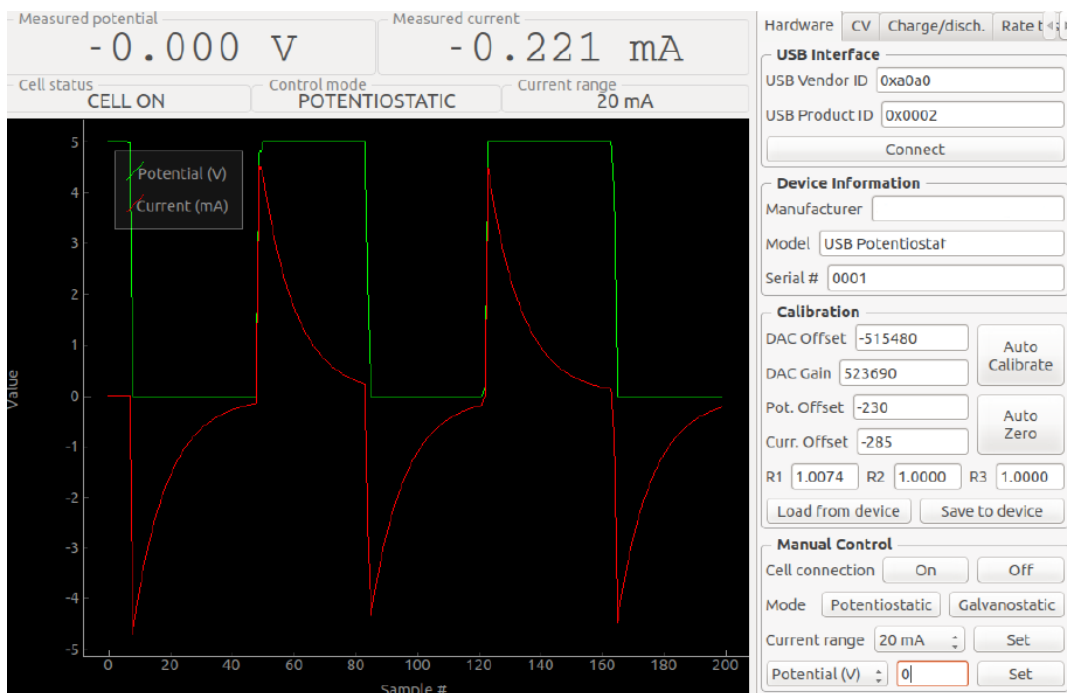


Figure 6.1: Current and potential measurement example (adapted from [24]).

6.2.2. CV measurement

As it was explained, CV measurement is a versatile electrochemical measurement technique, but it is essentially based on the repeated application of a linear potential ramp in the format of the triangular waveform while measuring the resulting current. In the typical CV graphic, the current is then plotted as a function of the applied potential. [24]

Before the beginning of the CV measurement, are set some parameters in the user interface program, Node-RED, a graphic example is in Figure 6.2.

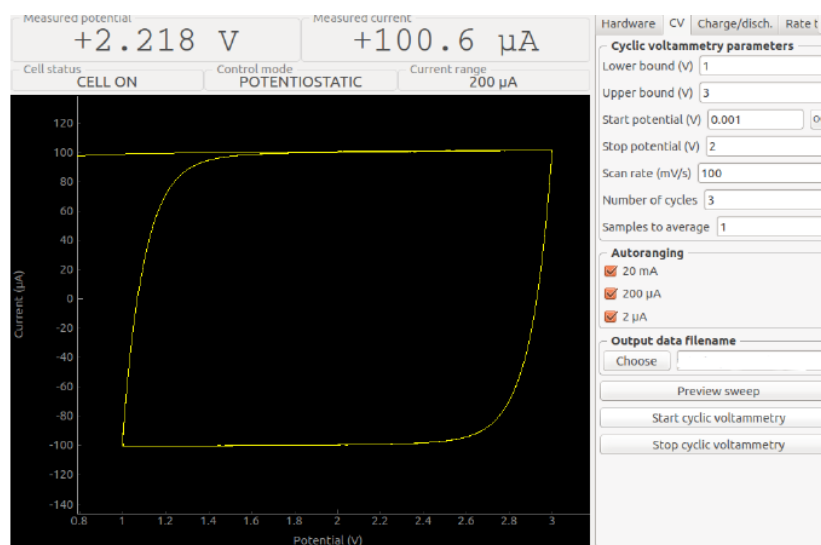


Figure 6.2: CV measurement example (adapted from [24]).

These parameters determine the nature of the applied triangular waveform and are graphically illustrated in Figure 6.3.

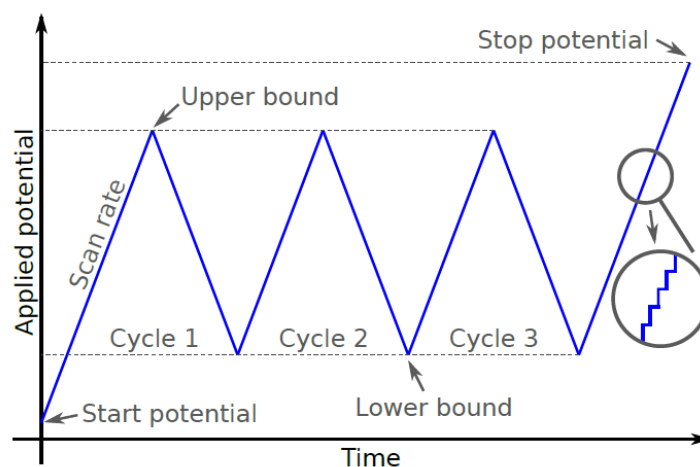


Figure 6.3: Triangular waveform (adapted from [24]).

Because of the finite resolution, step size, and potential and time, the waveform is not really linear but consists of a staircase shape. However, when the steps are sufficiently small, the results are equivalent to a truly linear ramp.

6.2.3. Charge/discharge measurement

Another commonly used electrochemical technique is to apply a constant current and to observe the evolution of the measured potential over time. In analytical redox chemistry, this method is known as coulometric titration. [24]

In the field of battery research, it can be used to determine the capacity of electrode material. Using the galvanostatic mode of the potentiostat, such a measurement technique is easily implemented. Figure 6.4 shows a charge and discharge measurement running on the dummy cell.

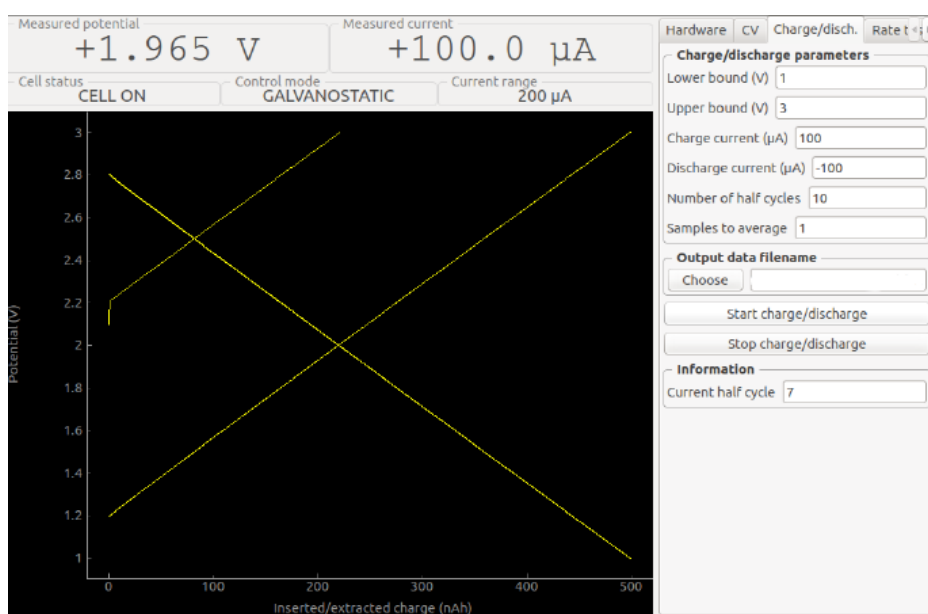


Figure 6.4: Charge/Discharge measurement example (adapted from [24]).

Chapter 7

7. Conclusions

The main objective of this dissertation was to perform an electrochemical study of MFCs reactors with a low-cost potentiostat. The primary issue with the potentiostat application was that there wasn't possible to achieve the controlled environment of the MFCs reactors in time, so the dissertation has become a theoretical application instead of a practical one.

It was concluded that the potentiostat brings many advantages in its usage for the MFCs studies. Produces extreme low noise and controls currents from femtoamperes to kiloamperes. It is usually a certain amount of noise. To reach a high power potentiostat, there is no point to measure extremely small currents with it. But within limits, potentiostats are versatile instruments. So, the advantages of potentiostat are mainly that it is fast and low noise.

7.1. Future work

The two primary next steps for this project entail the reactivation of MFCs reactors and the completion of the potentiostat PCB components assembly, such as the extern ADC and DAC. With these steps working, the aim is to perform the electrochemical tests with the reactors.

To have more accurate results and an elaborated discussion, laboratory tests with a traditional potentiostat should be made, to have reference results and compare the tradicional potentiostat with the low-cost potentiostat. Besides this objective, it could be added more parameters to the study of MFCs, adding more tests in the protocol established.

Bibliography

- [1] W. V. and K. R. Bruce E. Logan, Bert Hamelers, René Rozendal, Uwe Shroder, Jurg Keller, Stefano Freguia, Peter Aelterman, "Critical Review Microbial Fuel Cells : Methodology and Technology," *Environ. Sci. Technol.*, vol. 40, no. 17, pp. 5181–5192, 2006, [Online]. Available: <http://pubs.acs.org/doi/abs/10.1021/es0605016>.
- [2] B. E. Logan, *Microbial Fuel Cells*. Hoboken, New Jersey: John Wiley & Sons, 2008.
- [3] "MFC - Documents by year." <https://www.scopus.com> (accessed Oct. 05, 2020).
- [4] C. Santoro, C. Arbizzani, B. Erable, and I. Ieropoulos, "Microbial fuel cells: From fundamentals to applications. A review," *J. Power Sources*, vol. 356, pp. 225–244, 2017, doi: 10.1016/j.jpowsour.2017.03.109.
- [5] B. E. Logan and J. M. Regan, "Microbial fuel cells - Challenges and applications," *Environ. Sci. Technol.*, vol. 40, no. 17, pp. 5172–5180, 2006, doi: 10.1021/es0627592.
- [6] A. S. Mathuriya, D. A. Jadhav, and M. M. Ghangrekar, "Architectural adaptations of microbial fuel cells," *Appl. Microbiol. Biotechnol.*, vol. 102, no. 22, pp. 9419–9432, 2018, doi: 10.1007/s00253-018-9339-0.
- [7] F. Zhao, R. C. T. Slade, and J. R. Varcoe, "Techniques for the study and development of microbial fuel cells: An electrochemical perspective," *Chem. Soc. Rev.*, vol. 38, no. 7, pp. 1926–1939, 2009, doi: 10.1039/b819866g.
- [8] J. Li, "An Experimental Study of Microbial Fuel Cells for Electricity Generating: Performance Characterization and Capacity Improvement," *J. Sustain. Bioenergy Syst.*, vol. 03, no. 03, pp. 171–178, 2013, doi: 10.4236/jsbs.2013.33024.
- [9] E. S. Friedman, M. A. Rosenbaum, A. W. Lee, D. A. Lipson, B. R. Land, and L. T. Angenent, "A cost-effective and field-ready potentiostat that poises subsurface electrodes to monitor bacterial respiration," *Biosens. Bioelectron.*, vol. 32, no. 1, pp. 309–313, 2012, doi: 10.1016/j.bios.2011.12.013.
- [10] P. Theodosiou, "Optimisation of Microbial Fuel Cells (MFCs) through bacterial-robot interaction," p. 208, 2019.
- [11] I. A. Ieropoulos *et al.*, "Pee power urinal-microbial fuel cell technology field trials in the context of sanitation," *Environ. Sci. Water Res. Technol.*, vol. 2, no. 2, pp. 336–343, 2016, doi: 10.1039/c5ew00270b.
- [12] *Potentiostats*. German: Bank Elektronik - Intelligent controls GmbH.
- [13] A. V. Gopinath and D. Russell, "An Inexpensive Field-Portable Programmable Potentiostat," *Chem. Educ.*, vol. 6, no. 05, pp. 1–6, 2005.

- [14] N. Elgrishi, K. J. Rountree, B. D. McCarthy, E. S. Rountree, T. T. Eisenhart, and J. L. Dempsey, "A Practical Beginner's Guide to Cyclic Voltammetry," *J. Chem. Educ.*, vol. 95, no. 2, pp. 197–206, 2018, doi: 10.1021/acs.jchemed.7b00361.
- [15] A. j. Bard and L. R. Faulkner, *Electrochemical methods: Fundamentals and Applications*, Second., vol. 677, no. 1. 2004.
- [16] C. C. Yang, "Recovery of heavy metals from spent Ni-Cd batteries by a potentiostatic electrodeposition technique," *J. Power Sources*, vol. 115, no. 2, pp. 352–359, 2003, doi: 10.1016/S0378-7753(03)00015-6.
- [17] K. Kellner, T. Posniecek, J. Ettenauer, K. Zuser, and M. Brandl, "A new, low-cost potentiostat for environmental measurements with an easy-to-use PC interface," *Procedia Eng.*, vol. 120, no. December, pp. 956–960, 2015, doi: 10.1016/j.proeng.2015.08.820.
- [18] J. Aymerich *et al.*, "Cost-effective smartphone-based reconfigurable electrochemical instrument for alcohol determination in whole blood samples," *Biosens. Bioelectron.*, vol. 117, no. April, pp. 736–742, 2018, doi: 10.1016/j.bios.2018.06.044.
- [19] P. Bemnowicz, G. Z. Yang, S. Anastasova, A. M. Spehar-Délèze, and P. Vadgama, "Wearable electronic sensor for potentiometric and amperometric measurements," *2013 IEEE Int. Conf. Body Sens. Networks, BSN 2013*, no. 1, pp. 2–6, 2013, doi: 10.1109/BSN.2013.6575531.
- [20] Y. C. Li *et al.*, "An Easily Fabricated Low-Cost Potentiostat Coupled with User-Friendly Software for Introducing Students to Electrochemical Reactions and Electroanalytical Techniques," *J. Chem. Educ.*, vol. 95, no. 9, pp. 1658–1661, 2018, doi: 10.1021/acs.jchemed.8b00340.
- [21] R. Rossi, D. Pant, and B. E. Logan, "Chronoamperometry and linear sweep voltammetry reveals the adverse impact of high carbonate buffer concentrations on anode performance in microbial fuel cells," *J. Power Sources*, vol. 476, no. July, p. 228715, 2020, doi: 10.1016/j.jpowsour.2020.228715.
- [22] B. E. Logan *et al.*, "Impact of Ohmic Resistance on Measured Electrode Potentials and Maximum Power Production in Microbial Fuel Cells," *Environ. Sci. Technol.*, vol. 52, no. 15, pp. 8977–8985, 2018, doi: 10.1021/acs.est.8b02055.
- [23] F. Zhang *et al.*, "Reference and counter electrode positions affect electrochemical characterization of bioanodes in different bioelectrochemical systems," *Biotechnol. Bioeng.*, vol. 111, no. 10, pp. 1931–1939, 2014, doi: 10.1002/bit.25253.
- [24] T. Dobbelaere, P. M. Vereecken, and C. Detavernier, "A USB-controlled potentiostat/galvanostat for thin-film battery characterization," *HardwareX*, vol. 2, pp. 34–49, 2017, doi: 10.1016/j.ohx.2017.08.001.

- [25] T. Instruments and I. Sbas, “Low-Power , Rail-to-Rail Output , 16-Bit Serial Input DIGITAL-TO-ANALOG CONVERTER,” no. June, 2003.
- [26] S. Ads, “ANALOG-TO-DIGITAL CONVERTERS with Serial Interface ADS8331,” no. December 2009, 2012.
- [27] T. Instruments and I. Slls, “ISO724x High-Speed , Quad-Channel Digital Isolators OUTx,” 2015.
- [28] B. Aremo, M. Oyebamiji Adeoye, I. B. Obioh, and O. A. Adeboye, “A Simplified Microcontroller Based Potentiostat for Low-Resource Applications,” *Open J. Met.*, vol. 05, no. 04, pp. 37–46, 2015, doi: 10.4236/ojmetal.2015.54005.
- [29] P. M. D. Serra, A. Espírito-Santo, and M. Magrinho, “A steady-state electrical model of a microbial fuel cell through multiple-cycle polarization curves,” *Renew. Sustain. Energy Rev.*, vol. 117, no. July 2019, p. 109439, 2020, doi: 10.1016/j.rser.2019.109439.
- [30] K. Ferencz and D. József, “Using Node-RED platform in an industrial environment.,” no. February, p. 13, 2020.
- [31] U. S. B. Otg, “Rapid prototyping for the LPC1768 MCU.”
- [32] E. Embedded and S. Design, *Chapter 7: Starting with Serial Communication*. 2016.
- [33] Z. He, S. D. Minter, and L. T. Angenent, “Electricity generation from artificial wastewater using an upflow microbial fuel cell,” *Environ. Sci. Technol.*, vol. 39, no. 14, pp. 5262–5267, 2005, doi: 10.1021/es0502876.
- [34] L. M. Tender *et al.*, “The first demonstration of a microbial fuel cell as a viable power supply: Powering a meteorological buoy,” *J. Power Sources*, vol. 179, no. 2, pp. 571–575, 2008, doi: 10.1016/j.jpowsour.2007.12.123.